Melanization of *Candida auris* is Associated with Alteration of Extracellular pH

Daniel F. Q. Smith[‡1], Nathan J. Mudrak[‡1,2], Daniel Zamith-Miranda[‡3,4], Leandro Honorato[5], Leonardo Nimrichter [5], Barbara Smith[6], Gary Gerfen[7], Joshua D. Nosanchuk[#3,4], Arturo Casadevall[#1]

[1] W. Harry Feinstone Department of Molecular Microbiology and Immunology, The Johns Hopkins Bloomberg School of Public Health, Baltimore, MD, USA
[2] Krieger School of Arts & Science, Johns Hopkins University, Baltimore, MD, USA
[3]Department of Microbiology and Immunology, Albert Einstein College of Medicine, Bronx, New York, USA
[4]Division of Infectious Diseases, Department of Medicine, Albert Einstein College of Medicine, Bronx, New York, USA
[5] Laboratório de Glicobiologia de Eucariotos, Departamento de Microbiologia Geral, Instituto de Microbiologia, Universidade Federal do Rio de Janeiro, Rio de Janeiro, Brazil
[6] Institute for Basic Biomedical Sciences Microscope Facility, The Johns Hopkins School of Medicine, Baltimore, MD, USA
[7] Department of Biochemistry, Albert Einstein College of Medicine, Bronx, New York, USA

[‡] DFQS, NJM, and DZM contributed equally to this work
[#] JDN and AC contributed equally to this work

Abstract

Candida auris is a recently emerged global fungal pathogen, which causes life threatening infections, often in healthcare settings and with immunocompromised patients. *C. auris* infections are particularly worrisome because the fungus is often resistant to multiple classes of antifungal drugs. Furthermore, the fungus forms durable biofilms that are difficult to remove from surfaces. Due to the relatively recent, resilient, and resistant nature of this fungal pathogen, we investigated whether *C. auris* made common fungal virulence factor melanin. Melanin is a black-brown pigment that enables microbes to evade the mammalian immune response due to its strong antioxidant properties, ability to inactivate antimicrobial peptides, shielding of pathogen-associated molecular patterns, and inactivation of antifungal drugs. We found that certain strains of *C. auris,* predominantly from Clade I and IV, oxidized catecholamines into melanin pigment. The formation of this melanin occurred extracellularly, resulting in granule-like melanin structures that are deposited on the surface of the fungus. This melanization was primarily chemically driven and mediated by alkalinization of the extracellular environment. The *C. auris* strains had relatively high cell surface hydrophobicity, but we did not find a correlation between hydrophobicity and ability to melanize. Melanin protected the fungus from oxidative damage but we did not observe a protective role *in vitro* or *in vivo* during infection of macrophages or *Galleria mellonella*, respectively. In summary, *C. auris* alkalinizes the extracellular medium, which promotes the chemical autooxidation of the L-dopa to melanin that then attaches to its surface, thus illustrating a different mechanism for fungal melanization.

Introduction

Candida auris is an emerging fungal pathogen that is believed to original in marine wetlands and marshes (1,2). *C. auris* was first described in a clinical setting in 2009, but patient samples have been retrospectively determined to be *C. auris* as early as 1996 (3–5). Since its discovery, *C. auris* has caused outbreaks in at least 47 countries (3). *C. auris* is often acquired in healthcare settings and is believed to cause infections via biofilms formed on medical equipment and intravenous catheters leading to bloodstream infection (candidemia) and dissemination to organs (6). *C. auris* is further notable because it has a remarkably high resistance to known antifungal therapies, with exceedingly high resistances to azole and echinocandin classes of antifungal drugs (3,7). This poses a major concern for clinicians treating infections, as the fungus may be resistant to many of the commonly used antifungal therapeutics. Hence, a deeper understanding is needed about the physical properties of *C. auris* and how they contribute to virulence.

One unexplored aspect of *C. auris* physiology is whether it can produce the virulence factor melanin. Other *Candida* species, such as *C. albicans* and *C. glabrata* produce this virulence factor (8–11). Melanin is a black-brown, insoluble, acid resistant pigment found throughout a plethora of life forms, and has particular importance in the context of fungal virulence in mammals (12,13). In fungi, melanin is typically produced through either the oxidation of catecholamines (DOPA melanin), the tyrosine degradation pathway (pyomelanin), or through polyketide synthase pathways (DHN melanin) (12). Genes controlling melanization are affected by temperature, nutrient stress and copper/metal ion concentration (14–16), and the biochemical processes can be altered by the environmental antioxidant balance and pH (17,18). Melanin is formed either within the cell in organelles termed “melanosomes” and then exported to the cell wall, or in the cell wall itself (19,20). Once located within the cell wall the pigment is typically anchored through interactions with chitin, chitosan, and other cell wall components (9,21,22). Melanin strongly interacts with polysaccharides, lipids, and proteins, many of which are still intact following boiling in acid, lipid extraction, and enzymatic degradation, and fungi are thought to use these molecules as a scaffold for the melanin deposition in the cell wall (19,23,24). This melanin could also be secreted, as seen in *C. neoformans,* where melanin granules are shed from the cell wall and can be recovered from the supernatant (19,25).

Functionally, fungal melanin pigments have strong antioxidant properties that allow them to resist oxidative damage caused by the host immune cells, such as macrophage and neutrophil oxidative bursts (26). Additionally, melanin can bind and sequester antimicrobial peptides and antimicrobial enzymes that the host typically use to degrade and kill fungi during infection, as well as antifungal drugs used to treat infections (27–29). Fungal melanins located in the cell wall can alter cell wall composition and affect recognition of pathogen-associated molecular patterns that would otherwise be exposed. This may lead to diminished recognition by host immune cells. Conversely, DHN melanin can be recognized by the melanin sensing C-type lectin (MelLec) receptor, which is part of the human innate immune response, and can enhance fungal clearance (30). Melanin could also be presented to lymphocytes in a stimulatory context, which results in melanin-specific antibody production, which can inevitably lead to fungal opsonization, phagocytosis, and complement deposition (27,31,32).

In this study, we investigated the ability of 18 *C. auris* strains to produce melanin. Like other fungi, we found that *C. auris* produces a black melanin pigment, which was located on the surface of the cell wall. However, we found that, unlike other fungi, the melanization occurs extracellularly, in the supernatant. In liquid culture, the cell-free melanin can adhere to the surface of the cell and cause pigmentation of the fungus. We found this process to be mediated by the *C. auris'* ability to neutralize the pH of the media it is grown in, resulting in enhanced autoxidation of the catecholamine melanin substrate. This method of melanin production differs greatly from what is reported in other fungi. *C. auris* melanin

protected the fungus from oxidative stress but was not protective *in vitro* in the context of interactions with macrophages, or in an *in vivo* challenge of *Galleria mellonella* larvae.

Results

Temperature Dependence of *Candida auris* Strain Melanization

To evaluate the ideal temperature for *Candida auris* melanization, we tested the degree of melanization at both 30° and 37 °C. We found that the strains melanized to a greater extent at the higher temperature compared to the lower temperature (Figure 1A-C). The melanin-capable strains of *C. auris* were CDC 385, CDC 386, CDC 387, CDC 388, CDC 389, CDC 390, CDC 931, CDC 1097, CDC 1104, and MMC1. Strain CDC 382 exhibited an intermediate melanin phenotype. Additionally, we note that certain strains, namely CDC 388, CDC 390, CDC 1097, and MMC1 melanized significantly more at 37 °C and not at the lower temperature. This has interesting implications for understanding regulation of melanization and the role it has in warm environmental niches, as well as during infections of humans, who have a normal core body temperature of ~37 ˚C.

Further, the capacity of individual strains to melanize was associated with their evolutionary clade, with strains belonging to clades I and IV – associated with South Asia and South America, respectively – demonstrating melanization activity, while those strains belonging to clades II and II – associated with East Asia and Africa, respectively – did not. In addition, the single representative of clade V – associated with Iran – melanized, but the lack of additional clade V isolates for testing hinders the generalization of this finding.

Electron paramagnetic resonance (EPR)

Melanin generally contains a stable free-radical, which lends to its antioxidant properties. Stable free radical species can be detected by electron paramagnetic resonance (EPR). Melanin from 7-days cultures was extracted from 12 strains of *C. auris* and analyzed by EPR, with melanin extracted from *C. neoformans* H99 used as a standard (Figure 1D-F). The EPR spectra from the non-melanizing strains did not display the melanin-distinctive EPR peak (Figure 1E), but the EPR spectra from the pigment extracted from the melanin-producing strains (Figure 1F) were similar to the spectrum obtained from *C. neoformans* melanin (Figure 1D).

Time and Cell Density

To understand the optimal conditions for melanin production by *C. auris*, yeast cells were incubated with L-DOPA starting with different cell densities, and the production of pigment was analyzed for 13 days and compared to cells incubated in the absence of L-DOPA (Figure 2). *C. neoformans* was also cultivated with the same conditions and compared to the *C. auris* melanization profile. Melanin production was optimal by cells in high density (10^7 cells/mL). In this condition, melanin was visible from day 3, and intensified along the days, reaching its peak between days 7 and 10. Some strains melanized in a delayed fashion when in medium cell density (10^6 cells/mL), whereas none of the low density (10^5 cell/mL) cultures produced visible pigment. The cell density-associated phenotype presented by *C. neoformans* was the opposite of that presented by *C. auris*, as melanin production by low cell density *C. neoformans* cells was equally or more effective than in the high-density conditions.

Candida auris Strains Melanize Using Substrates Associated with DOPA melanin

We examined various known melanin precursors to evaluate which the *C. auris* strains could use as substrates for melanization, and if there are any strain-specific differences between the substrates used. We found that at a starting inoculum of 10^7 cells/ml, melanin-capable *C. auris* strains were able to use L-3,4-dihydroxyphenylalanine (L-DOPA), D-3,4-dihydroxyphenylalanine (D-DOPA), L-methyl-3,4-

137 dihydroxyphenylalanine (Methyl-DOPA/M-DOPA), dopamine, norepinephrine, epinephrine, and a mixture
138 of catecholamine neurotransmitters (dopamine, epinephrine, and norepinephrine) at the ratios found in
139 the mammalian brain (33). We found that in general, all melanin-capable *C. auris* strains were able to use
140 the same substrates (Figure 3A). Some strains, namely CDC 385 and CDC 386 were less able to
141 produce pigment when grown with dopamine. While the L-DOPA, D-DOPA, M-DOPA, dopamine, brain
142 mix, and norepinephrine produced dark brown-black pigments, the epinephrine produced a reddish-brown
143 amber color of melanization (Figure 3B).
144 Notably, the *C. auris* strains were unable to use L-tyrosine, homogentisic acid (HGA), and 4-
145 hydroxyphenylpyruvic acid (4-HPP) as precursors to melanization, which indicates that *C. auris* cannot
146 produce pyomelanin, a process typically mediated by laccases (34), and does not have a tyrosinase
147 enzyme that can convert L-tyrosine into suitable catecholamine melanin precursors. Additionally, the
148 strains are unable to oxidize ABTS, a laccase-specific substrate, further indicating that the melanization
149 agent is not a laccase (Figure 3C).
150
151 **Melanin is Primarily Found in the Supernatant**
152 During collection of the melanized cells, we noted that the supernatants of the cultures were
153 notably darker than expected given our work with another melanizing fungus, *C. neoformans* (Figure 4A,
154 B). Similarly, when cells were grown on agar plates with L-DOPA as a substrate for melanization, there
155 was a distinct halo of pigment surrounding the melanin-producing strains of *C. auris (*Figure 4C). Notably,
156 there was little to no pigmentation of the yeast colony itself. This strongly indicated that the melanization
157 of the cells was primarily extracellular and did not originate within the cells themselves.
158 To evaluate whether the supernatant of the cells had melanin-producing enzymatic activity, we
159 added L-DOPA to the isolated supernatant. We found that the supernatants of melanizing strains, namely
160 the supernatant of MMC1, CDC 387 (B8441), and CDC 388 (B11098), were capable of oxidizing L-
161 DOPA, whereas the supernatant of non-melanizing strain CDC 381 (B11220) and minimal media alone
162 were not. This indicates, in part, that the melanin-producing components of the *C. auris* were secreted
163 (Figure 4D).
164 Using ultracentrifugation, we collected small particles and extracellular vesicles found within the
165 melanized supernatant of the liquid cultures. We found that a substantial amount of the pigment was in
166 this supernatant pellet. Using negative staining transmission electron microscopy (TEM), we found that
167 the pelleted melanin was within granule structures, comparable to what was seen in the cell wall
168 periphery of the melanized culture (Figure 4E, F). These structures measured 20-40 nm (Figure 4E), and
169 were similar in appearance to melanin granules secreted by *C. neoformans* (19). The granules from CDC
170 381 had the smallest mean diameter (~20 nm) and CDC 387 had the largest at ~40 nm (Figure 4F).
171
172 **Cell-bound Melanin is localized to the Periphery of the Cell Wall**
173 To visualize the localization of melanin on the *C. auris* cells grown in liquid media, we used light
174 microscopy, TEM, and scanning electron microscopy (SEM). Under light microscopy, dark pigmentation
175 of the cells appeared to be located primarily in the cell wall, with infrequent additional intracellular
176 pigmentation, possibly due to oxidation of L-DOPA within a large vacuole (Figure 5A). Comparing TEM
177 micrographs of melanized and non-melanized cultures, we saw electron-dense structures found
178 exclusively in the melanized cultures that primarily appeared on the periphery of the cell wall. These
179 electron-dense structures are likely melanin granules and appeared to be rounded and granular. The
180 extracellular melanin granules also appeared unbound to the cell wall (Figure 5B). These extracellular
181 melanin granules were similar to the secreted melanin granules that were roughly 20-40 nm in diameter
182 (Figure 5B, 4E-F). Similarly, samples imaged with SEM showed that melanized cells had raised structures

183 on their surface, indicative of the structures observed in TEM (Figure 5C). Further, in the case of CDC
184 387, 388, and MMC1, the melanin granules appear to hold the cells together in large, aggregated clumps.
185 To determine whether the directionality of the cell-bound melanin deposition (i.e., if melanization
186 occurred in the cell wall and then was released into media, or if melanization occurred primarily in the
187 media and then attached to the cell wall periphery), we performed a series of add-back experiments, in
188 which we added melanized supernatant to the cells from the same *C. auris* strain grown without L-DOPA.
189 We found that the cells become pigmented by three hours of incubation with the melanized supernatant
190 (Figure 6A-D). Additionally, when we added melanized supernatant from the CDC 388 strain to the non-
191 melanizing CDC 381 strain, the CDC 381 strain accumulated pigment (Figure 6D). First, since CDC 381
192 cannot readily produce pigment, this showed that the pigment accumulation in these add-back
193 experiments was due to adhesion of the already synthesized pigment in the supernatant rather than the
194 production of new pigment from unreacted L-DOPA in the supernatant. Second, it indicated that the
195 melanin-deficient cells did not have a cell wall difference that made them intrinsically unable to bind
196 extracellular melanin. These add-back experiment data, along with the secretion data in Figure 4 and
197 Figure 5, point to the conclusion that *C. auris* cell wall melanization occurs extracellularly and then sticks
198 to the outside of the cell wall.
199 We grew CDC 387 and CDC 388 with L-DOPA in the presence of compounds known to enhance
200 or block the proper formation of cell wall components (9,35), either through direct supplementation of the
201 cell wall components, by binding and blocking proper structure formation, or by inhibiting the enzyme
202 responsible for producing that cell wall component. This allowed us, in theory, to evaluate which
203 components of the cell wall were important for extracellular melanin adherence. Cultures conditions that
204 resulted in a darker supernatant than the control condition indicated the lack of melanin adherence to the
205 cell wall, and those with lighter supernatant indicated that the compound enhanced melanin adherence to
206 the cell wall.
207 Addition of N-acetylglucosamine (GlcNAc) enhances the cell wall's layer of chitin and also
208 increases cell wall melanization in *C. neoformans* and *C. albicans* (9,36). In CDC 387 and CDC 388,
209 addition of 5 mM GlcNAc did not enhance cell wall melanin adhesion, and resulted in darker supernatant,
210 perhaps indicating less adhesion (Figure 6E, F). In TEM micrographs, the melanin located in the cell wall
211 between the control and GlcNAc treated did not appear appreciably different (Figure 6G, H).
212 Conversely, we added 100 μM Calcofluor White (CFW), which forms hydrogen bonds with chitin
213 polymers as they grow and thus disrupts proper formation of chitin microfibrils (37,38). Adding this dye led
214 to markedly decreased supernatant pigmentation (Figure 6E, F). Intriguingly, under microscopic analysis,
215 the CFW appeared to precipitate and form crystals that bound the melanin. The adhesion of melanin to
216 the CFW crystals was the likely cause of the lack of pigmented supernatant. This resulted in black
217 crystals that had the fluorescent properties of the CFW, along with the expected CFW-stained cell walls
218 (Supplementary Figure 1A). The CFW crystals were also visible under electron microscopy (Figure 6H,
219 Supplementary Figure 1B). The crystallization persisted despite filter sterilization. In an assay with cell-
220 free supernatant with CFW and with/without L-DOPA, we confirmed that the melanin formed bound to the
221 CFW crystals and precipitated out of solution (Supplementary Figure 1C). We also noticed that the CDC
222 387 and CDC 388 strain supernatants without L-DOPA form a smaller population of CFW crystals
223 compared to the CDC 381 non-melanizing strains (Supplementary Figure 1D). This finding may indicate
224 that there is a correlation between the melanization factor and formation of CFW crystal fragments with a
225 smaller size, which could indicate better solubility.
226 Further, we grew the CDC 387 and CDC 388 strains under the presence of the antifungal
227 compound caspofungin at half of the inhibitory concentration reported by the Centers for Disease Control
228 and Prevention (CDC) (37), which inhibits the enzymes responsible for cell wall β-glucan synthesis.
229 Caspofungin treatment resulted in high levels of supernatant melanization (Figure 6E, F). Under light

230 microscopic and electron microscopic analysis, the treatment appeared to reduce the amount of melanin
231 present on the cell wall, with nearly no melanin visible on the cell wall via TEM (Figure 6G, H).
232 Additionally, in the CDC 388 strain, caspofungin treatment resulted in what appeared to be pseudohyphal
233 growth (Supplementary Figure 1E). Although the cells were able to grow in culture under this
234 concentration of caspofungin, in the electron micrograph, the cells appeared to have a deformed
235 morphology, and their cytoplasmic contents looked condensed and abnormal, potentially due to the
236 antifungal stress and cell wall defect (Figure 6G, H).
237
238 **Melanization Affects the Hydrophobicity of Some *C. auris* Strains**
239 Since melanin is a hydrophobic molecule, we investigated whether melanization had a correlation
240 with the cell surface hydrophobicity (CSH) of the *C. auris* strains. With *C. auris* strains grown in the
241 nutrient rich Yeast Peptone Dextrose (YPD) media and minimal media, 7 of 12 strains had CSH that was
242 greater than 80% (Figure 6I, J). There was no association between the strain hydrophobicity and its ability
243 to melanize, as the strongly melanizing strain CDC 387 and the weak/no melanizing strains CDC 381 and
244 MMC2 all had low hydrophobicity. Conversely, the non-melanizing strains CDC 383 and melanizing
245 strains CDC 388 had high hydrophobicity. Additionally, since hydrophobicity is known to play roles in
246 host-pathogen interactions (38–40), we investigated whether melanization affected the CSH of the *C.*
247 *auris* strains. Surprisingly, we found in the CDC 387 strain (and to a lesser extent in the non-melanizing
248 strain CDC 381), growth in L-DOPA for 7 days resulted in decreased CSH compared to the controls
249 grown without L-DOPA (Figure 6K). In CDC 388 and MMC1, we did not see a change in CSH following
250 melanization, although these strains had notably high levels of hydrophobicity at ~90%.
251
252 **Supernatant Melanization is Resistant to Denaturing Conditions**
253 To further elucidate the identity of the melanin-producing components, we sought to characterize
254 properties and constraints on supernatant melanization. We first assessed the supernatant's melanization
255 activity after exposure to high temperatures. We observed a modest reduction in the supernatant's
256 capacity to melanize after a 1 h incubation at 100˚C, and no significant difference between the
257 melanization activity of the precipitate or supernatant that formed after boiling (Figure 7A). After treating
258 samples with the serine proteinases Trypsin or Proteinase K, we assessed the supernatant melanization
259 activity and observed no reduction in the capacity for melanization (Figure 7B-D). Further, melanization
260 activity was unaffected by treatment with 1% w/v SDS or methanol; however, melanization was increased
261 after treatment with 6 M Urea in all conditions, indicating the urea affected the melanization reaction
262 irrespective of the melanizing strain-specific factor in the supernatant (Figure 7E). These observations
263 argue against the melanization factor being a protein.
264 We sought to characterize the size of the melanin-producing components. After passing the
265 supernatant with a 3 kDa protein cut-off filter, we found that melanization activity was partially conserved
266 in the flowthrough of the concentrator, suggesting that the melanization factor was not larger than 3 kDa.
267 To check whether a melanin-producing component was being protected from denaturation within
268 EVs, we treated supernatant with Triton X-100 and SDS in combination with proteinases. If the
269 melanization factor was protected within EVs, adding detergent will disturb the EV integrity and allow the
270 protease to degrade the protein contents within (41–43). We did not find that EVs protect a melanizing
271 factor from proteolytic degradation (Figure 7G). This was further supported by a lack of enriched
272 melanization activity observed in an EV-enriched ultracentrifuged pellet (Supplementary Figure 2).
273
274 **Melanization Genes in the *C. auris* Genome**
275 We searched the C. auris genome of enzymes that have been associated with melanin synthesis
276 in other fungi such as laccases, phenol oxidases and tyrosinases. We found a number of hypothetical

277 multicopper oxidase and ferroxidase genes reported in the *C. auris* genome. However, we have no
278 evidence that these have laccase or tyrosinase-like functions and appear similar to metal ion transporters,
279 peroxisomal membrane components, and ergosterol synthesis (Supplementary Table 1 and 2). Hence,
280 the absence of tyrosinase and laccase activity in *C. auris* corresponds with the absence of a clearly
281 identifiable enzyme in the genome.
282
283 **Supernatant Neutral pH Correlated with *C. auris* Strains' Abilities to Melanize**
284 Due to the smaller crystal size of the CFW in the supernatants from the melanizing strain, we
285 measured the pH of the supernatants since alkaline pH can enhance the solubility of CFW solutions
286 (44,45). Additionally, the urea treatment, which produced an alkaline environment, increased supernatant
287 melanization in all the strains. We found a strong correlation between the pH of the conditioned media
288 and the degree to which the cultures melanized (Figure 8A). We found that the melanizing strains have a
289 supernatant of around 6.5, whereas the non-melanizing strains tended to have a supernatant closer to pH
290 5.75. This change in pH was in the range in which L-DOPA and other catecholamines auto-oxidize to
291 melanin (Figure 8B).
292 We altered the supernatants' pHs to be either pH 5.5 or 7 by adding hydrochloric acid or
293 potassium hydroxide. We found that melanization activity was halted at pH 5.5, including the
294 supernatants of CDC 387 and CDC 388, but was enhanced at pH 7 (Figure 8C, D). Most notably, the
295 supernatant from CDC 381 – a non-melanizing strain – gained melanization activity at higher pH to an
296 extent statistically indistinguishable from that of the melanizing strains – CDC 387 and CDC 388 at the
297 same pH. This strongly suggests that the pH of the supernatant was a major contributor to the
298 extracellular melanization activity observed.
299 As endogenous production of ammonia has been reported in *C. albicans* under stress conditions
300 (46), we assessed the ammonia concentrations of supernatants using a commercially available
301 colorimetric assay that specifically detects ammonia (47). We observed higher ammonia concentrations in
302 supernatants from *C. auris* strains that melanized and had higher pH (Figure 8E,F).
303 We collected the oxidized L-DOPA from the supernatants of CDC 381, CDC 387, and CDC 388,
304 and minimal media alone at their baseline pH (~5.75, 6.5, 6.5, and 5.5, respectively) and at pH 7. We
305 imaged these melanized particles using negative staining TEM. Interestingly, we found that the melanized
306 particles from CDC 387 and CDC 388 had structural differences compared with the oxidized L-DOPA in
307 the minimal media at pH 7 (Figure 8G). The particles collected from the supernatant with oxidized L-
308 DOPA were similar to those collected from cultures, whereas the oxidized L-DOPA in minimal media
309 alone had smaller particles, rougher clumps of electron dense material (Figure 8G). This suggested that
310 there is some component in the supernatant that may help in structuring the auto-polymerized L-DOPA,
311 by acting as a scaffold, which allows it to form spherical and linear structures like beads on a string.
312 Melanin is known to strongly bind to carbohydrates, lipids, and proteins, which may be factors (19,23).
313
314 **Melanin Protects *C. auris* from Oxidative Damage**
315 *C. auris* cultures incubated, or not, with L-DOPA for 7 days were treated with hydrogen peroxide
316 (H_2O_2) and yeast viability was evaluated (Figure 9A). The incubation with H_2O_2 reduced the viability of all
317 evaluated strains of *C. auris*. The melanin-producing strains (CDC 387 and CDC 388) incubated with L-
318 DOPA were partially protected from the H_2O_2, when compared to cells from the same strain grown in the
319 absence of L-DOPA. Strain CDC 381 showed similar viability in the presence and in the absence of L-
320 DOPA, indicating that melanin protects *C. auris* yeast cells against oxidative attack by H_2O_2.
321
322 **Melanin Does Not Protect *C. auris* Against Macrophage Killing**

323 Melanized and control *C. auris* yeast cells were incubated with bone marrow-derived
324 macrophages (BMDM) for 2 and 24 hours and yeast killing was addressed. In the tested conditions
325 melanin did not confer protection to the yeast cells against macrophage killing (Figure 9B). It was
326 interesting to observe that whereas the killing in 2 hours was similar among the strains, in 24 hours CDC
327 381 was shown to be partially resistant against macrophage killing, as opposed to the susceptible
328 phenotype showed by strains CDC 387 and CDC 388.
329
330 **Melanin Does Not Affect *C. auris* Virulence During *Galleria mellonella in vivo* Infection**
331 Larvae of *G. mellonella* were infected with yeast cells from melanized and control *C. auris* and
332 survival was evaluated. As seen for the killing experiment with mouse macrophages, the presence of
333 melanin did not impact the survival of *Galleria mellonella* larvae (Figure 9C), suggesting that melanization
334 of *C. auris* prior to infection did not confer protection to the fungus in this invertebrate model.
335
336 **Discussion:**
337 In this paper, we have investigated the ability of *C. auris* to produce melanin, a multifunctional
338 pigment found across biology and in many pathogenic fungi. Some of the functions of melanin include the
339 ability to neutralize reactive oxygen species during immune activation, inactivate antimicrobial peptides,
340 and inactivate antifungal drugs (12,13,48). Due to these immune and treatment evasive properties, our
341 findings that *C. auris* can melanize may have clinical relevance, particularly in regard to our
342 understanding of how this fungus is treated.
343 We evaluated the ability of sixteen *C. auris* strains to melanize when grown in the presence of L-
344 DOPA, a common melanin substrate. We found that most strains melanized, manifested by darkening of
345 cultures, and that the ability to melanize was enhanced at higher temperatures (37˚C compared to 30˚C).
346 We had anticipated that melanization would occur similarly in all strains, so it was surprising that only
347 some strains had the ability to melanize. Further, based on our understanding of fungal melanization, we
348 expected melanization to occur more at 30˚C rather than 37˚C, as it does in other fungi such as
349 *Cryptococcus neoformans (49).* This also has relevancy for pathogenesis in humans, as human body
350 temperature is 37˚C and thus more conducive to ideal *C. auris* melanization conditions. Interestingly, the
351 pattern of melanization correlated with the clade in which the strain belonged to; *C. auris* strains from
352 Clade I and IV, which are associated with South Asia and South America, respectively, are the melanizing
353 strains, while the non-melanizing strains are from Clade II and III, which are typically associated with East
354 Asia and South Africa, respectively. This could point to some lineage-specific genetic or epigenetic
355 differences that are responsible for the melanization phenotype or regulating the melanization process.
356 Another aspect that differed from the pigmentation observed in other fungi was the impact of cell density
357 on melanization by *C. auris*. We observed that melanization in *C. auris* required high cell density (10^7
358 cells/mL). However, at an intermediate cell density (10^6 cells/mL) only some strains of *C. auris* (CDC 382,
359 385, 386, and 389) were able to produce melanin in a delayed fashion. This observation could indicate
360 the need of a quorum sensing molecule to trigger effective melanization in *C. auris*.
361 In addition, we tested the substrate specificity of the melanizing abilities of *C. auris.* We found that
362 *C. auris* produces melanins consistent with typical DOPA-melanins using catecholamine substrates such
363 as L-DOPA, D-DOPA, Methyl-DOPA, dopamine, epinephrine, and norepinephrine. *C. auris* was unable to
364 produce melanin from L-Tyrosine indicating there is no tyrosinase present, nor are there enzymes
365 capable of producing pyomelanin from a tyrosine degradation pathway. The *C. auris* genome has
366 hypothetical genes related to tyrosinase, but these genes appear more related to ergosterol synthesis or
367 magnesium/zinc ion transport. Similarly, *C. auris* was unable to form pyomelanin from homogentisic acid
368 (HGA) and 4-hydroxyphenylpyruvic acid (4-HPP). Laccases, such as those in *C. neoformans*, are able to
369 produce pyomelanin from HGA (34). These results in *C. auris* would suggest that a laccase does not exist

370 as it does in *C. neoformans,* or at least not one with as much of a wide-ranging substrate range.
371 Melanization in other DOPA-melanin producing fungi is often catalyzed by laccases (50) or multicopper
372 ferroxidases (11). Current annotation of the *C. auris* genome indicate there are hypothetical laccases,
373 oxidoreductase, and ferroxidases (Ontology Groups OG6_100257 and OG6_100380), however these
374 appear to be related to metal ion homeostasis and part of the peroxisomal membrane. Since we do not
375 know the function or expression pattern of these hypothetical genes, we cannot rule out that they are
376 capable of oxidizing catecholamines under certain conditions. However, our evidence points to a non-
377 laccase, non-tyrosinase, and general non-enzymatic mechanism as the responsible melanin-producing
378 factor.
379 We investigated the cellular localization of the melanin in three selected *C. auris* strains: CDC
380 381 which is a non-melanizing strain, CDC 387 which is a strongly melanizing strain, and CDC 388 which
381 is a moderately melanizing strain that mostly produces pigment at 37˚C. For some experiments, we
382 included the MMC1 strain that, like CDC 388, is a moderately melanizing strain. Using light microscopy,
383 we observed numerous dark aggregates on the outside of the melanized CDC 388, MMC, and particularly
384 CDC 387 cells, which tended to have a fluffy appearance and appeared in between areas where cells
385 were clumped together. In addition, the cells themselves appeared darker, and some had large
386 intracellular melanized spots which would appear to correspond to a vacuole. Based on our evidence that
387 melanization occurs extracellularly due to the alkalinization of the supernatant, we believe these dark
388 spots within the vacuole were due to L-DOPA autoxidation within the vacuole following storage under
389 nutrient-deprived conditions. In the CDC 381 strain, these features were minimal to non-existent. To
390 further gain understanding of the melanin on an ultrastructural level, we used TEM and SEM. In essence
391 we found that there were electron dense spherical structures on the surface of the melanized *C. auris,*
392 which were bound to the outermost layer of the cell wall or were associated with the cell wall. These
393 structures were only present in melanized cells, and were consistent with previously reported melanin
394 granules (9,19). Interestingly, these structures were not reliably seen intracellularly, and were significantly
395 smaller than the extracellular melanin structures seen during *C. albicans* melanization (9). The CDC 387
396 cells had a distinct phenotype where there were many multivesicular bodies (MVBs) within the cell and
397 merging with the plasma membrane, resulting in secretion of extracellular vesicles. Using SEM, we also
398 saw the presence of these spherical particles on the surface of the melanized *C. auris* strains, especially
399 the CDC 387 strains where the surface was heavily decorated in these structures.
400 One notable observed feature of the heavily melanized *C. auris* CDC 387 strain is that it tended
401 to form large aggregates of cells, which were melded together by extracellular melanin, as indicated by
402 light and electron microscopy. This aggregation is notable, as aggregation is a known physical property in
403 some strains of *C. auris,* outside of the context of melanin. The aggregate phenotype has been
404 hypothesized to function as a way for the fungus to remain within tissues and evade immune clearance,
405 and may play a role in biofilm formation and maintenance (51–53). If melanization is inducing a sort of
406 aggregative phenotype as our data suggests, this could have similar implications in understanding the
407 role of *C. auris* melanin in pathogenesis.
408 We that the supernatant of the melanized cultures were quite dark, particularly in the CDC 388
409 and MMC1 strains, which indicated there was secreted melanin. We also see this on solid agar, where all
410 the melanizing strains had a halo of melanin around the colonies and the non-melanizing strains do not.
411 The strongly melanizing strains CDC 385, CDC 386, CDC 387, and CDC 389 have the darkest halos of
412 melanin surrounding the colonies. The fungal colonies themselves remain white with no change in
413 pigmentation by 7 days of growth. The notion that the melanin is extracellular and secreted is supported
414 by the TEM and SEM which show melanized structures on the surface of the cells. Using negative
415 staining TEM of the isolated melanin from the supernatant, we see melanin granules similar to those seen
416 in TEM of whole cells, where the CDC 387 granules are the largest, followed by MMC1 and CDC 388.

417 The CDC 381 granules were the smallest and fewest. When we added the melanized supernatant to non-
418 melanized cells, including to CDC 381, we found that the melanin adhered to the cells and made the
419 appearance of a melanized cell pellet. These findings indicated that the extracellular melanin could
420 adhere to the outside of the cell wall and suggested that melanization occurred externally and aggregates
421 of the polymer adhere to the cell wall. It also shows that the CDC 381 cell wall is conducive to
422 melanization and its lack of melanization activity is not due to an inherent deficiency of the cell wall. When
423 L-DOPA was added to the cell-free supernatant of the cultures, we see that the supernatant from CDC
424 388 and CDC 387 had melanizing activity whereas the supernatant from CDC 381 did not, again,
425 indicating that the component responsible for melanization was extracellular.
426 To determine the extracellular factor responsible for melanization, we did a series of assays on
427 the cell-free supernatant. First, we determined that the melanization factor was stable at 100˚C, was
428 resistant to proteolytic degradation by trypsin and Proteinase K and was smaller than 3 kDa. These
429 observations together indicated that the melanization component was not a protein, but was likely a small
430 molecule. Further, the melanizing ability of the supernatant is not enriched in the extracellular vesicles
431 collected through ultracentrifugation, nor is it protected by EVs. We cannot exclude the possibility that
432 EVs are used as scaffolding for the melanization, as previously found in *C. neoformans* (54). However,
433 melanization activity is not lost after treatment with methanol, urea, nor SDS detergents.
434 Interestingly, we found that the ability for a strain to melanize correlated directly to the pH of the
435 supernatant within minimal media, where non-melanizing strains had a supernatant ~5.75 and melanizing
436 strains had a pH ~6.5. This strong correlation also corresponds to the steep increase in autoxidation of L-
437 DOPA between those pH ranges. We additionally found that artificially adjusting the pH of the
438 supernatant to pH 7 makes all the supernatants melanize, whereas adjusting the pH to 5.5 prevented all
439 the supernatants from melanizing, even the supernatants from the melanizing strains. These data
440 suggest that the melanization is due to the ability of some strains to alter the acidity of surrounding
441 environment more than others. We find strong evidence that this ability to neutralize the media was due to
442 the production of ammonia by some of the strains. Fungi, including *C. albicans* and *C. neoformans,* are
443 known to produce ammonia to help persist under pH stress (46,55,56). *C. auris* has been found in
444 environmental reservoirs within marine saltwater marshes (2). Microbes found in marine wetland
445 environmental niche are faced with alkaline stress and, as a result, may be naturally more alkaliphilic
446 (57).
447 L-DOPA autoxidation is highly dependent on pH (17,18). L-DOPA has an isoelectric point of pH
448 6.0, meaning that at pH 6 or above, the L-DOPA is more likely to have a deprotonated amine group,
449 which results in more energetically favorable oxidation, cyclization, and dopachrome formation (18). While
450 autoxidation of catecholamines could occur in the absence of any fungus, we found that the oxidized L-
451 DOPA from the supernatant of the *C. auris* strains had a different structure than the autoxidized L-DOPA
452 from the minimal media alone at a neutral pH. This indicated that there are some properties of the
453 supernatant that encourage the autoxidized L-DOPA to organize into specific spherical structures. Based
454 on previous understanding of how melanin interacts with other biological molecules, we hypothesize this
455 melanin scaffold to be polysaccharide, protein aggregates, or perhaps even lipids. The structure of the
456 melanin polymer around this scaffolding could change its biophysical properties. This could account for
457 one reason why there is significantly more melanin associated with the CDC 387 strain – the strain
458 changes the pH of the supernatant significantly, but the electron micrographs also show the cells have a
459 large amount of multivesicular bodies and organelles fusing with the plasma membrane, which would
460 indicate a relative hypersecretion of polysaccharides, proteins, and extracellular vesicles. Interestingly,
461 the supernatant of the non-melanized CDC 387 strain has a yellow tint to it, which indicates that some
462 molecules are being released in higher amounts compared with the CDC 381 and CDC 388 strains.

463 This pH-based mechanism of fungal melanization differs greatly from other ways in which fungi
464 produce melanin, including *C. albicans* (9–11). In *C. albicans,* melanization is mediated by ferroxidases, a
465 class of enzymes that are genetically similar to the melanin-producing enzyme laccase in *C. neoformans.*
466 The knockout of some ferroxidase genes (*FET* genes) results in a loss of melanization phenotype.
467 We found that the *C. auris* strains, generally, were remarkably hydrophobic, with most strains' cell
468 surface hydrophobicity (CSH) being in the 90-100% range. Comparatively, the CSH of clinical isolates of
469 *C. albicans* strains ranges from about 2 to 41% (38). In *C. albicans,* CSH is reportedly associated with
470 increased adhesion to epithelial cells, biofilm formation, resistance to neutrophil-mediated killing, and
471 increased overall virulence (39,58–60). These findings have implications for studying how *C. auris*
472 interacts with hydrophobic surfaces, and how hydrophobicity may contribute to durable biofilm formations
473 within hospital environments and medical equipment. We do not find an association between CSH and
474 ability of the strain to melanize. Since melanin is a hydrophobic polymer, we anticipated that melanization
475 of cultures would enhance CSH. Surprisingly, we found that growth in minimal media with L-DOPA
476 reduced the hydrophobicity of the non-melanizing strain CDC 381 and the strong melanizing strain CDC
477 387, while the CSH of CDC 388 and MMC1 were virtually unchanged. We hypothesize that the
478 hydrophobic melanin is comparatively less hydrophobic than the hydrophobicity-mediators on the surface
479 of the *C. auris* cells, and when the melanin binds to the cell wall, it results in the relative decrease of CSH.
480 In *C. albicans,* CSH is believed to be mediated by exposure of hydrophobic cell wall mannoproteins
481 (40,61), which could correspond to areas in which melanin is deposited (62).
482 The antioxidant properties of melanin are partially responsible for its protective properties (63).
483 Melanized *C. auris* yeast cells were partially protected against hydrogen peroxide, and this protection was
484 stronger in the strain where melanization is more efficient (CDC 387). This observation is in accordance
485 with the expected properties of melanin pigments (12,48). However, melanin did not confer any protection
486 to *C. auris* in an *in vitro* challenge with BMDM. The *in vitro* killing of *C. auris* by BMDM was tested at
487 distinct times and, in the evaluated conditions, melanin played no role on protecting the fungus from the
488 phagocytes. The previously described degree of protection from killing, conferred by melanin to
489 pathogenic fungi varies considerably (18 % to > 36 %) (64), so it is possible that the pattern observed for
490 *C. auris* is similar to the one of *C. albicans*, where there is not a clear association between melanin and
491 virulence (9). Supporting the *in vitro* findings, *in vivo* experiments using the invertebrate *G. mellonella*,
492 showed that melanin produced by *C. auris* might not protect the fungus against innate immunity, but we
493 cannot rule out a potential action of melanin in interfering in processes that lead to acquired immunity.
494 In summary, we found that Clade I, IV, and V strains of *C. auris* grown with catecholamine
495 substrates produce melanin extracellularly by alkalinizing the media with ammonia, which promoted non-
496 enzymatic catecholamine oxidation. This extracellular melanin aggregates and binds to the outside of the
497 *C. auris* cell wall (Summarized in Figure 12). While we did not find evidence that the melanin formed by *C.*
498 *auris* interferes with the effector mechanisms of innate immune cells, nor is it an active melanization
499 process, our findings leave open the possibility that environment alkalinization could be a new
500 mechanism by which fungi can drive the production of melanin. It is also possible that melanization may
501 play a role in the environmental survival of *C. auris*, where the fungus is likely to encounter oxidative
502 stressors. Not much is known about the environmental niche of *C. auris,* however, the first environmental
503 isolates have been uncovered and described in the marine marshlands off the Andaman Islands in India
504 (2).
505
506 **Materials and Methods**
507
508 ***Candida auris* strains and media**

509 All isolates of *Candida auris* strains were received from the Centers of Disease Control and Prevention
510 Food and Drug Administration Antimicrobial Resistance Isolate Bank
511 (https://wwwn.cdc.gov/arisolatebank/Panel/PanelDetail?ID=2), with the exceptions of MMC1 and MMC2,
512 which were previously described clinical isolates (65). CDC 381 is also known as B11220, CDC 387 is
513 also known as B8441, and CDC 388 is also known as B11098. All *C. auris* strains were first grown in
514 Yeast Peptone Dextrose (YPD) broth at 30°C until they reached stationary phase. Cultures were washed
515 twice and put into Minimal Media (15.0 mM glucose, 10.0 mM $MgSO_4$, 29.4 mM KH_2PO_4, 13.0 mM
516 glycine, 3.0 M vitamin B_1, pH 5.5) at 37°C at 10^7 cells/ml unless otherwise noted. Cells were grown for 7
517 days under continuous shaking.
518
519 ***C. auris* Melanization in Liquid Media**
520 All *C. auris* strains were grown in minimal media as described above, with the addition of melanin
521 precursors to be tested. All compounds used for the melanization substrate assay and ABTS (2,2'-azino-
522 bis(3-ethylbenzothiazoline-6-sulfonic acid) laccase assay were prepared in concentrated stock solutions
523 and added to the culture at a final concentration of 1 mM except for caspofungin, which was added at 0.5
524 μg/ml final concentration. For the experiments evaluating the temperature dependence of the *C. auris*
525 strain melanization, cultures were also grown at 30˚C for 7 days in minimal media. After 7 d, cultures were
526 scanned with a CanoScan9000F scanner at 600 dpi. Mean Gray Value for each well of culture was
527 determined using the Measure tool on FIJI image processing software (66).
528
529 Experiments where cultures were grown on solid agar petri dishes, 20 μl of stationary washed culture
530 were added to minimal media agar with 1 mM of 3,4, Dihydroxyl-L-phenylalanine (L-DOPA). Plates were
531 incubated at 37˚C for 7 days and imaged with a scanner CanoScan9000F at 600 dpi.
532
533 **Melanin extraction and electron paramagnetic resonance (EPR)**
534 Melanin was extracted from selected strains of *C. auris* and one strain of *C. neoformans* (H99) as
535 described (67). Briefly, after growing for 7 days in minimal medium containing L-DOPA (1 mM), cells were
536 washed with sorbitol/sodium citrate solution, and incubated with Novozyme 234 for 1 hour at 30˚C.
537 Samples were incubated with guanidine thiocyanate for 1 hour, followed by an incubation with HCl 6 M.
538 After boiling the solution for 1 hour, the pellets were washed and suspended in PBS. Extracted melanin
539 was submitted to EPR. The EPR spectra of the collected dark particles were registered using a Varian
540 E112 X-Band model spectrometer with a TE102 resonator and a liquid nitrogen finger Dewar. The EPR
541 runs were performed under the following parameters that are similar to our fungal melanin studies as
542 previously described (8): modulation frequency of 100 kHz, modulation amplitude of 1.6 G, center field of
543 3,310 G, sweep width of 100.0 G, microwave frequency of 9.2 GHz, microwave power of 1.0 mW, time
544 constant of 0.5 s, and temperature of 77 K .
545
546 **Extracellular Melanin Isolation**
547 Cultures grown for 7 days with or without L-DOPA as a substrate for melanization were centrifuged at
548 4,000 x *g* for 5 minutes. The supernatant was removed and filter sterilized through a 0.8 μm syringe filter
549 (Corning, Corning, NY). To measure the melanization of the supernatant, absorbance measurements
550 were performed at 492 nm using a SpectraMax iD5 spectrophotometer. For experiments collecting and
551 analyzing the extracellular melanin particles, the supernatants were then ultracentrifuged at 100,000 x *g*
552 for 1 hour at 4°C in a Beckman Coulter Optima L-90K UltraCentrifuge. Supernatants were decanted and
553 the melanized pellet was suspended in PBS.
554

555 **Supernatant Melanization Activity**
556 To assess phenoloxidase activity of the supernatant, L-DOPA was added to cell-free supernatant from
557 non-melanized cultures. Subsequently, the supernatant was left to incubate for 72 hours at 37° C in
558 darkness. Activity was determined through SpectraMax iD5 spectrophotometer readings at 492 nm taken
559 at 0 and 72 hours and images were taken using the CanoScan9000F flatbed scanner at a resolution of
560 600 dpi. For the proteinase assays, supernatants were pre-treated with 1:10 Trypsin (Corning) at 37˚C, or
561 with approximately 200 μg/ml Proteinase K (New England BioLabs) at 60˚C prior to the addition of L-
562 DOPA. To measure the degree of protection conferred by extracellular vesicles against degradation of
563 potential melanin-producing components, supernatants were pre-treated with 0.01% w/v SDS or 0.1% v/v
564 Triton X-100 (Sigma) with or without Proteinase K. Supernatants were then incubated for one hour at
565 60˚C as described. Heat degradation assays were performed by heating supernatant samples to 100˚C
566 for one hour prior to testing for melanization activity.
567
568 **Light Microscopy**
569 *C. auris* strains were imaged using light microscopy using an Olympus AX70 microscope and 100x
570 objective.
571
572 **Transmission Electron Microscopy (TEM)**
573 *C. auris* melanized and non-melanized cells were imaged using TEM as described (25). Briefly, samples
574 2% (w/v) glutaraldehyde in 0.1 M cacodylate at room temperature for 2 h, followed by overnight
575 incubation in 4% (w/v) formaldehyde, 1% (w/v) glutaraldehyde, and 0.1% PBS overnight at 4 °C.
576 Samples were washed, fixed with 1% osmium tetroxide for 90 minutes, washed with dH_2O, serially
577 dehydrated in ethanol, and embedded in SPURRS resin. Thin sections, 60 to 90 nm, were cut with a
578 diamond knife on the Leica Ultracut E Ultramicrotome and picked up with 2x1 mm formvar coated copper
579 slot grids. Grids were stained with 2% uranyl acetate (aq) and 0.4% lead citrate before imaging on a
580 Hitachi 7600 TEM at 80 kV. Images were captured with an AMT XR80 CCD (8 megapixels, 16
581 bit). Secreted melanin was visualized using negative staining, in which 8 μl of sample was placed on a
582 negative glow discharged 400 mesh ultra-thin carbon-coated grids (EMS CF400-CU-UL) for 30 s,
583 followed by three quick rinses of Tris-buffered Saline (TBS) and staining with 2.5% uranyl acetate.
584 Samples were imaged using a Hitachi 7600 TEM Electron Microscope at 80 kV. Images were captured
585 with an AMT XR80 CCD (8 megapixels, 16 bit). Following image acquisition, diameter measurements of
586 the secreted melanin particles were performed using the measurement tool of FIJI image processing
587 software (66).
588
589 **Scanning Electron Microscopy (SEM)**
590 Briefly, samples were fixed in 2.5% (v/v) glutaraldehyde in 0.1 M sodium phosphate buffer (pH 7.3)
591 overnight at 4 °C. Samples were placed on a poly-L-lysine coated coverslip (0.01 mg/ml , coated for 5
592 minutes, and rised twice in dH2O) for 1 hour, then washed, serially dehydrated in ethanol, chemically
593 dried using hexamethyldisilazane (HMDS) and dried overnight in a desiccator. Samples were then placed
594 on a metal sample stub (EMS aluminum 6mm pin, 12.7 mm diameter) with double sided carbon tape
595 (EMS standard carbon adhesive tabs, 12 mm Diameter) and the underside of the coverslip coated with
596 silver paint (EMS silver conductive coating). Samples were coated with 15 nm gold palladium (AuPd), on
597 a Denton Desk III sputter coater before imaging on a ThermoFisher Helios FIB-SEM at 5 kV using an Ion
598 Conversion and Electron (ICE) detector.
599
600 **Extracellular Melanin Add-back**

601 Cell-free melanized supernatant was added to a pellet of non-melanized cells from the same
602 corresponding strain of *C. auris.* Samples were mixed at 37°C for 3 h and pelleted at 4,000 x *g* for 5
603 minutes. Pelleted cells were image compared to control cells treated for 3 hours with the non-melanized
604 supernatant.
605
606 **Cell Wall Disruption Assays**
607 All cultures were grown in minimal media for 7 days with 1 mM L-DOPA. In addition to the L-DOPA, either
608 5 mM N-acetylglucosamine (GlcNAc) (9,35), 100 μg/ml Calcofluor White (9,35), or 50% MIC of
609 Caspofungin based on the CDC resistance profile (37) (Antibiotic Resistance Isolate Bank, Centers for
610 Disease Control and Prevention, Atlanta, GA, USA) was added to the culture at the beginning of the 7 d
611 incubation. Cultures were collected after 7 d, and supernatant and cells were examined under light and
612 electron microscopy as described above.
613
614 **pH Measurements and Supernatant pH Alteration**
615 Cultures were grown for 7 days in minimal media at 37˚C. Cultures were centrifuged at 4,000 *x* g for 4
616 minutes, and supernatant was filter sterilized with a 0.22 μm PES Filter (Millipore-Sigma). Supernatant pH
617 was determined using a calibrated Fisher Scientific Accumet AB150 pH meter.
618
619 Cell-free supernatants were isolated, and their pH measured using a calibrated Fisher Scientific Accumet
620 AB150 pH meter. Samples were split into three groups: unaltered supernatant, supernatant manually
621 adjusted to pH 5.5 with hydrochloric acid (HCl), and supernatant manually adjusted to pH 7 with
622 potassium hydroxide (KOH). Titrations with HCl and KOH were performed using the same pH meter set to
623 continuously read pH. Each sample's three groups were then treated with 1 mM L-DOPA and incubated
624 at 37˚C for 72 hours in darkness. Melanization activity was determined through SpectraMax iD5
625 spectrophotometer readings at 492 nm and images were taken using the CanoScan9000F flatbed
626 scanner at a resolution of 600 dpi.
627
628 **Ammonia Quantification**
629 Supernatant ammonia concentration was quantified using the commercially available API Ammonia Test
630 Kit (API) according to manufacturer's protocol, with test solution volumes scaled down in proportion to the
631 small volumes tested to maintain the established test solution concentrations. A standard curve of
632 ammonia concentrations from 16 ppm to 0.25 ppm was constructed by serial diluting 28% ammonium
633 hydroxide (Sigma) in PBS to enable validation of this modification and colorimetric correlation to known
634 ppm values. In a 48-well plate, 1 drop of both solutions 1 and 2 were added to 625 μl of cell-free
635 supernatant, after which the plate was agitated and left to sit for 5 minutes with a lid on. The color
636 change, from yellow to dark blue-green during the formation of indophenol blue dye, was quantified by
637 reading 680 nm absorbance using a SpectraMax iD5 spectrophotometer. In addition, plates were imaged
638 at 600 dpi using the CanoScan9000F flatbed scanner.
639
640 **Cell Surface Hydrophobicity**
641 Cell surface hydrophobicity was measured by Microbial Adhesion to Hexadecane (MATH) assay as
642 described (68). Briefly, cells were resuspended in PBS to an optical density of 0.2 - 0.4 at 600 nm using
643 SpectraMax iD5 spectrophotometer. This was measured in triplicate and recorded as the initial value. 3
644 mL of cells in PBS were added to a glass test tube followed by 400 μl of n-hexadecane. Tubes were
645 parafilmed and vortexed on high for 45 seconds each and left to settle for 2 minutes. Aliquots of the
646 aqueous (bottom) layer were carefully removed, and the absorbance at 600 nm was measured as the
647 final value. Hydrophobicity was calculated as: 100*(Initial Value – Final Value)/(Initial Value).

648
649 **Oxidative stress**
650 Yeast cells grown in the presence, or absence, of L-DOPA for 7 days at 37 °C were incubated in RPMI
651 medium buffered with MOPS, containing or not, hydrogen peroxide (H_2O_2) 5mM for 3 hours at 37 °C
652 under shaking. Cell suspensions were diluted and plated onto Sabouraud-agar plates for colony-forming
653 units (CFU) counting. The cytotoxic effect of H_2O_2 in each strain was calculated as the number of yeast
654 cells in the presence of H_2O_2, divided by the yeast count in the absence of H_2O_2, multiplied by 100 to be
655 expressed as percentage.
656
657 **Killing by bone marrow-derived macrophages**
658 Bone marrow cells isolated from C57BL/6 mice were cultivated in RPMI containing 10% of FBS and 20%
659 of L929 supernatant for 7 days with media addition on day 3. At the end of the differentiation time, cells
660 were plated in 96-well plates (10^5 cells per well) and incubated at 37 °C for adherence. Macrophages
661 were challenged with *C. auris* (0.5 x 10^5 yeast cells per well), grown in the presence or the absence of L-
662 DOPA (1mM). In parallel, *C. auris* was added to wells in the same conditions but without macrophages.
663 After 2 or 24 h, the plates were centrifuged, the supernatant discarded, and the pellets were suspended in
664 sterile distilled H_2O. The suspensions were diluted and plated onto Sabouraud-agar plates and incubated
665 at 30 °C for 24 h for CFU counting. For each experimental group, the percentage of yeast killing was
666 calculated as: yeast + macrophage group divided by yeast in the absence of macrophages.
667
668 ***Galleria mellonella* infection**
669 Groups of 10 insects (250-300 mg) in the final instar larval stage were used. Larvae were injected with
670 melanized or non-melanized yeasts of *C. auris* (2 x 10^6 cells in 10 μL) into the haemocoel through the last
671 left pro-leg strains using a Hamilton syringe. For these experiments the strains CDC 381, CDC 387 and
672 CDC 388 were selected. PBS was used as a control. The insects were then placed in sterile Petri dishes
673 and maintained in the dark at 37 °C. The numbers of living larvae were monitored twice daily and
674 recorded for a period of 7 days. Larvae were considered dead if no response to physical stimulus was
675 observed.
676
677 **Bioinformatics Search of Laccase and Tyrosinase Genes in *C. auris***
678 The keywords "laccase" and "tyrosinase" were searched separately in FungiDB.org. Results were filtered
679 and narrowed down to genes, and to those found in the taxonomic subset "[Candida] auris". Results were
680 then exported and downloaded as a comma-delineated file (.csv) including the following table columns:
681 Organism, GeneID, Product Description, Ortholog Group, EC numbers from OrthoMCL, Computed GO
682 Component IDs, Computed GO Components, Computed GO Function IDs, Computed GO Functions,
683 Computed GO Process IDs, Computed GO Processes, Interpro ID, Interpro Description, PFam ID, PFam
684 Description, Superfamily ID, and Superfamily Description.
685
686 **Acknowledgements:**
687 We would like to thank the Johns Hopkins University School of Medicine Microscope Facility for their
688 assistance with the electron microscopy experiments, and Rosanna Baker for her suggestions and
689 assistance with the ammonia experiments. We would also like to thank Dr. Christine Chrissian for her
690 helpful feedback during the writing process. The illustration in Figure 10 was made using Biorender.com.
691 DFQS, NM, and AC were supported by National Institute of Allergy and Infection Disease R01 AI052733,
692 R01 AI152078, and R01 AI052733. and the National Heart, Lung, and Blood Institute R01 HL059842.
693 D.F.Q.S. was funded by National Institutes of Health 5T32GM008752-18 and 1T32AI138953-01A1. The
694 funders had no role in study design, data collection and analysis, decision to publish, or preparation of the

manuscript. DZM and JDN were supported by National Institutes of Health (NIH)–National Institute of Allergy and Infectious Diseases grant R21 AI124797. LN and LH were supported by grants from the Brazilian agency Conselho Nacional de Desenvolvimento Científico e Tecnológico (CNPq; grants 311179/2017-7 and 408711/2017-7) and FAPERJ (E-26/202.809/2018).

References

1. Casadevall A, Kontoyiannis DP, Robert V. On the Emergence of Candida auris: Climate Change, Azoles, Swamps, and Birds. mBio [Internet]. 2019 Aug 27 [cited 2020 Sep 29];10(4). Available from: https://mbio.asm.org/content/10/4/e01397-19

2. Arora P, Singh P, Wang Y, Yadav A, Pawar K, Singh A, et al. Environmental Isolation of Candida auris from the Coastal Wetlands of Andaman Islands, India. mBio [Internet]. 2021 Mar 16 [cited 2022 Jan 23]; Available from: https://journals.asm.org/doi/abs/10.1128/mBio.03181-20

3. Ahmad S, Alfouzan W. Candida auris: Epidemiology, Diagnosis, Pathogenesis, Antifungal Susceptibility, and Infection Control Measures to Combat the Spread of Infections in Healthcare Facilities. Microorganisms. 2021 Apr;9(4):807.

4. Lee WG, Shin JH, Uh Y, Kang MG, Kim SH, Park KH, et al. First Three Reported Cases of Nosocomial Fungemia Caused by Candida auris. Journal of Clinical Microbiology [Internet]. 2011 Sep [cited 2022 Jan 24]; Available from: https://journals.asm.org/doi/abs/10.1128/JCM.00319-11

5. Satoh K, Makimura K, Hasumi Y, Nishiyama Y, Uchida K, Yamaguchi H. Candida auris sp. nov., a novel ascomycetous yeast isolated from the external ear canal of an inpatient in a Japanese hospital. Microbiol Immunol. 2009 Jan;53(1):41–4.

6. Horton MV, Nett JE. Candida auris infection and biofilm formation: going beyond the surface. Curr Clin Microbiol Rep. 2020 Sep;7(3):51–6.

7. Garcia-Bustos V, Cabanero-Navalon MD, Ruiz-Saurí A, Ruiz-Gaitán AC, Salavert M, Tormo MÁ, et al. What Do We Know about Candida auris? State of the Art, Knowledge Gaps, and Future Directions. Microorganisms. 2021 Oct 19;9(10):2177.

8. Almeida-Paes R, Figueiredo-Carvalho MH, da Silva LB, Gerfen G, S Araújo GR de, Frases S, et al. Candida glabrata produces a melanin-like pigment that protects against stress conditions encountered during parasitism. Future Microbiology. 2021 May 1;16(7):509–20.

9. Walker CA, Gómez BL, Mora-Montes HM, Mackenzie KS, Munro CA, Brown AJP, et al. Melanin Externalization in Candida albicans Depends on Cell Wall Chitin Structures. Eukaryotic Cell [Internet]. 2010 Sep [cited 2022 Jan 19]; Available from: https://journals.asm.org/doi/abs/10.1128/EC.00051-10

10. Morris-Jones R, Gomez BL, Diez S, Uran M, Morris-Jones SD, Casadevall A, et al. Synthesis of Melanin Pigment by Candida albicans In Vitro and during Infection. Infection and Immunity. 2005 Sep 1;73(9):6147–50.

11. Dai B, Xu Y, Gao N, Chen J. Wor1-regulated ferroxidases contribute to pigment formation in opaque cells of Candida albicans. FEBS Open Bio. 2021;11(3):598–621.

12. Smith DFQ, Casadevall A. The Role of Melanin in Fungal Pathogenesis for Animal Hosts. In: Rodrigues ML, editor. Fungal Physiology and Immunopathogenesis [Internet]. Cham: Springer International Publishing; 2019 [cited 2020 Sep 24]. p. 1–30. (Current Topics in Microbiology and Immunology). Available from: https://doi.org/10.1007/82_2019_173

737 13. Nosanchuk JD, Casadevall A. The contribution of melanin to microbial pathogenesis. Cellular
738 Microbiology. 2003;5(4):203–23.

739 14. Jiang N, Sun N, Xiao D, Pan J, Wang Y, Zhu X. A copper-responsive factor gene CUF1 is required
740 for copper induction of laccase in Cryptococcus neoformans. FEMS Microbiology Letters. 2009 Jul
741 1;296(1):84–90.

742 15. Mauch RM, Cunha V de O, Dias ALT. THE COPPER INTERFERENCE WITH THE
743 MELANOGENESIS OF *Cryptococcus neoformans*. Rev Inst Med trop S Paulo. 2013 Apr;55:117–
744 20.

745 16. Cordero RJB, Camacho E, Casadevall A. Melanization in Cryptococcus neoformans Requires
746 Complex Regulation. mBio [Internet]. 2020 Feb 4 [cited 2022 Jan 25]; Available from:
747 https://journals.asm.org/doi/abs/10.1128/mBio.03313-19

748 17. Chen Y chieh, Kendall T, Yip P, Davy A, Sefcik J, Sutter JU. Influence of Ions and pH on the
749 Formation of Solid- and Liquid-like Melanin. ACS Omega. 2020 Oct 6;5(39):25059–68.

750 18. Eslami M, Zare HR, Namazian M. Thermodynamic Parameters of Electrochemical Oxidation of l-
751 DOPA: Experimental and Theoretical Studies. J Phys Chem B. 2012 Oct 18;116(41):12552–7.

752 19. Camacho E, Vij R, Chrissian C, Prados-Rosales R, Gil D, O'Meally RN, et al. The structural unit of
753 melanin in the cell wall of the fungal pathogen Cryptococcus neoformans. Journal of Biological
754 Chemistry. 2019 Jul 5;294(27):10471–89.

755 20. Franzen AJ, Cunha MML, Miranda K, Hentschel J, Plattner H, da Silva MB, et al. Ultrastructural
756 characterization of melanosomes of the human pathogenic fungus Fonsecaea pedrosoi. Journal of
757 Structural Biology. 2008 Apr 1;162(1):75–84.

758 21. Baker LG, Specht CA, Donlin MJ, Lodge JK. Chitosan, the Deacetylated Form of Chitin, Is Necessary
759 for Cell Wall Integrity in Cryptococcus neoformans. Eukaryotic Cell [Internet]. 2007 May [cited 2022
760 Jan 24]; Available from: https://journals.asm.org/doi/abs/10.1128/EC.00399-06

761 22. Walton FJ, Idnurm A, Heitman J. Novel gene functions required for melanization of the human
762 pathogen Cryptococcus neoformans. Molecular Microbiology. 2005;57(5):1381–96.

763 23. Chrissian C, Camacho E, Kelly JE, Wang H, Casadevall A, Stark RE. Solid-state NMR spectroscopy
764 identifies three classes of lipids in Cryptococcus neoformans melanized cell walls and whole fungal
765 cells. Journal of Biological Chemistry. 2020 Oct 30;295(44):15083–96.

766 24. Chrissian C, Lin CPC, Camacho E, Casadevall A, Neiman AM, Stark RE. Unconventional
767 Constituents and Shared Molecular Architecture of the Melanized Cell Wall of C. neoformans and
768 Spore Wall of S. cerevisiae. Journal of Fungi. 2020 Dec;6(4):329.

769 25. Eisenman HC, Nosanchuk JD, Webber JBW, Emerson RJ, Camesano TA, Casadevall A.
770 Microstructure of Cell Wall-Associated Melanin in the Human Pathogenic Fungus Cryptococcus
771 neoformans. Biochemistry. 2005 Mar 1;44(10):3683–93.

772 26. Jacobson ES, Tinnell SB. Antioxidant function of fungal melanin. Journal of Bacteriology. 1993 Nov
773 1;175(21):7102–4.

774 27. Alviano DS, Franzen AJ, Travassos LR, Holandino C, Rozental S, Ejzemberg R, et al. Melanin from
775 Fonsecaea pedrosoi Induces Production of Human Antifungal Antibodies and Enhances the

776 Antimicrobial Efficacy of Phagocytes. Infection and Immunity [Internet]. 2004 Jan [cited 2022 Jan
777 24]; Available from: https://journals.asm.org/doi/abs/10.1128/IAI.72.1.229-237.2004

778 28. Doering TL, Nosanchuk JD, Roberts WK, Casadevall A. Melanin as a potential cryptococcal defence
779 against microbicidal proteins. Med Mycol. 1999 Jun;37(3):175–81.

780 29. Rosas ÁL, Casadevall A. Melanization decreases the susceptibility of Cryptococcus neoformans to
781 enzymatic degradation. Mycopathologia. 2001 Aug 1;151(2):53–6.

782 30. Stappers MHT, Clark AE, Aimanianda V, Bidula S, Reid DM, Asamaphan P, et al. Recognition of
783 DHN-melanin by MelLec, is required for protective immunity to Aspergillus. Nature. 2018 Mar
784 15;555(7696):382–6.

785 31. Nosanchuk JD, Rosas AL, Casadevall A. The Antibody Response to Fungal Melanin in Mice. The
786 Journal of Immunology. 1998 Jun 15;160(12):6026–31.

787 32. Rosas ÁL, Nosanchuk JD, Casadevall A. Passive Immunization with Melanin-Binding Monoclonal
788 Antibodies Prolongs Survival of Mice with Lethal Cryptococcus neoformans Infection. Infection and
789 Immunity [Internet]. 2001 May 1 [cited 2022 Jan 24]; Available from:
790 https://journals.asm.org/doi/abs/10.1128/IAI.69.5.3410-3412.2001

791 33. Baker RP, Chrissian C, Stark RE, Casadevall A. Cryptococcus neoformans melanization incorporates
792 multiple catecholamines to produce polytypic melanin. Journal of Biological Chemistry [Internet].
793 2022 Jan 1 [cited 2022 Jan 25];298(1). Available from: https://www.jbc.org/article/S0021-
794 9258(21)01329-6/abstract

795 34. Frases S, Salazar A, Dadachova E, Casadevall A. Cryptococcus neoformans Can Utilize the
796 Bacterial Melanin Precursor Homogentisic Acid for Fungal Melanogenesis. Applied and
797 Environmental Microbiology [Internet]. 2007 Jan [cited 2022 Jan 20]; Available from:
798 https://journals.asm.org/doi/abs/10.1128/AEM.01947-06

799 35. Perez-Dulzaides R, Camacho E, Cordero RJB, Casadevall A. Cell-wall dyes interfere with
800 Cryptococcus neoformans melanin deposition. Microbiology (Reading). 2018 Aug;164(8):1012–22.

801 36. Camacho E, Chrissian C, Cordero RJB, Liporagi-Lopes L, Stark RE, Casadevall A. N-
802 acetylglucosamine affects Cryptococcus neoformans cell-wall composition and melanin
803 architecture. Microbiology (Reading). 2017 Nov;163(11):1540–56.

804 37. Panel Details | Antimicrobial Resistance Isolate Bank | Antibiotic/Antimicrobial Resistance | CDC
805 [Internet]. [cited 2022 Jan 19]. Available from:
806 https://wwwn.cdc.gov/ARIsolateBank/Panel/PanelDetail?ID=2

807 38. Raut J, Rathod V, Karuppayil SM. Cell Surface Hydrophobicity and Adhesion: A Study on Fifty
808 Clinical Isolates of Candida albicans. Nippon Ishinkin Gakkai Zasshi. 2010;51(3):131–6.

809 39. Danchik C, Casadevall A. Role of Cell Surface Hydrophobicity in the Pathogenesis of Medically-
810 Significant Fungi. Frontiers in Cellular and Infection Microbiology [Internet]. 2021 [cited 2022 Jan
811 24];10. Available from: https://www.frontiersin.org/article/10.3389/fcimb.2020.594973

812 40. Krasowska A, Sigler K. How microorganisms use hydrophobicity and what does this mean for human
813 needs? Frontiers in Cellular and Infection Microbiology [Internet]. 2014 [cited 2022 Jan 24];4.
814 Available from: https://www.frontiersin.org/article/10.3389/fcimb.2014.00112

815 41. Wolf JM, Rivera J, Casadevall A. Serum albumin disrupts Cryptococcus neoformans and Bacillus
816 anthracis extracellular vesicles. Cell Microbiol. 2012 May;14(5):762–73.

817 42. Coelho C, Vij R, Smith DQ, Brady NR, Hamacher-Brady A, Casadevall A. Study of Microbial
818 Extracellular Vesicles:Separation by Density Gradients, Protection Assays and Labelling for Live
819 Tracking. Bio Protoc. 2020 Jan 20;10(2):e3502.

820 43. Coelho C, Brown L, Maryam M, Vij R, Smith DFQ, Burnet MC, et al. Listeria monocytogenes
821 virulence factors, including listeriolysin O, are secreted in biologically active extracellular vesicles. J
822 Biol Chem. 2019 Jan 25;294(4):1202–17.

823 44. Kim S, Inglett GE. Molecular weight and ionic strength dependence of fluorescence intensity of the
824 Calcofluor/β-glucan complex in flow-injection analysis. Journal of Food Composition and Analysis.
825 2006 Aug 1;19(5):466–72.

826 45. Wu J, Deng X, Tian B, Wang L, Xie B. Interactions between Oat β-Glucan and Calcofluor
827 Characterized by Spectroscopic Method. J Agric Food Chem. 2008 Feb 1;56(3):1131–7.

828 46. Vylkova S, Carman AJ, Danhof HA, Collette JR, Zhou H, Lorenz MC. The Fungal Pathogen Candida
829 albicans Autoinduces Hyphal Morphogenesis by Raising Extracellular pH. mBio [Internet]. 2011 Jul
830 1 [cited 2020 Sep 26];2(3). Available from: https://mbio.asm.org/content/2/3/e00055-11

831 47. Zadorojny C, Saxton S, Finger R. Spectrophotometric Determination of Ammonia. Journal (Water
832 Pollution Control Federation). 1973;45(5):905–12.

833 48. Liu S, Youngchim S, Zamith-Miranda D, Nosanchuk JD. Fungal Melanin and the Mammalian Immune
834 System. Journal of Fungi. 2021 Apr;7(4):264.

835 49. Jacobson ES, Emery HS. Temperature regulation of the cryptococcal phenoloxidase. Journal of
836 Medical and Veterinary Mycology. 1991 Jan 1;29(2):121–4.

837 50. Salas SD, Bennett JE, Kwon-Chung KJ, Perfect JR, Williamson PR. Effect of the laccase gene
838 CNLAC1, on virulence of Cryptococcus neoformans. J Exp Med. 1996 Aug 1;184(2):377–86.

839 51. Ben-Ami R, Berman J, Novikov A, Bash E, Shachor-Meyouhas Y, Zakin S, et al. Multidrug-Resistant
840 Candida haemulonii and C. auris, Tel Aviv, Israel. Emerg Infect Dis. 2017 Feb;23(2):195–203.

841 52. Rossato L, Colombo AL. Candida auris: What Have We Learned About Its Mechanisms of
842 Pathogenicity? Frontiers in Microbiology [Internet]. 2018 [cited 2022 Jan 20];9. Available from:
843 https://www.frontiersin.org/article/10.3389/fmicb.2018.03081

844 53. Bravo Ruiz G, Lorenz A. What do we know about the biology of the emerging fungal pathogen of
845 humans Candida auris? Microbiological Research. 2021 Jan 1;242:126621.

846 54. Eisenman HC, Frases S, Nicola AM, Rodrigues ML, Casadevall A. Vesicle-associated melanization
847 in Cryptococcus neoformans. Microbiology (Reading). 2009 Dec;155(Pt 12):3860–7.

848 55. Fu MS, Coelho C, Leon-Rodriguez CMD, Rossi DCP, Camacho E, Jung EH, et al. Cryptococcus
849 neoformans urease affects the outcome of intracellular pathogenesis by modulating
850 phagolysosomal pH. PLOS Pathogens. 2018 Jun 15;14(6):e1007144.

851 56. Vylkova S, Lorenz MC. Modulation of Phagosomal pH by Candida albicans Promotes Hyphal
852 Morphogenesis and Requires Stp2p, a Regulator of Amino Acid Transport. PLOS Pathogens. 2014
853 Mar 13;10(3):e1003995.

854 57. Meena B, Rajan LA, Vinithkumar NV, Kirubagaran R. Novel marine actinobacteria from emerald
855 Andaman & Nicobar Islands: a prospective source for industrial and pharmaceutical byproducts.
856 BMC Microbiol. 2013 Jun 22;13:145.

857 58. Singleton DR, Fidel PL Jr, Wozniak KL, Hazen KC. Contribution of cell surface hydrophobicity protein
858 1 (Csh1p) to virulence of hydrophobic Candida albicans serotype A cells. FEMS Microbiology
859 Letters. 2005 Mar 1;244(2):373–7.

860 59. Hazen KC, Brawner DL, Riesselman MH, Jutila MA, Cutler JE. Differential adherence of hydrophobic
861 and hydrophilic Candida albicans yeast cells to mouse tissues. Infection and Immunity [Internet].
862 1991 Mar [cited 2022 Jan 24]; Available from: https://journals.asm.org/doi/abs/10.1128/iai.59.3.907-
863 912.1991

864 60. Silva-Dias A, Miranda IM, Branco J, Monteiro-Soares M, Pina-Vaz C, Rodrigues AG. Adhesion,
865 biofilm formation, cell surface hydrophobicity, and antifungal planktonic susceptibility: relationship
866 among Candida spp. Front Microbiol [Internet]. 2015 [cited 2020 Sep 28];6. Available from:
867 https://www.frontiersin.org/articles/10.3389/fmicb.2015.00205/full?utm_source=newsletter&utm_me
868 dium=web&utm_campaign=Microbiology-w15-2015

869 61. Fukazawa Y, Kagaya K. Molecular bases of adhesion of Candida albicans. Journal of Medical and
870 Veterinary Mycology. 1997 Jan 1;35(2):87–99.

871 62. Tronchin G, Pihet M, Lopes-Bezerra LM, Bouchara JP. Adherence mechanisms in human pathogenic
872 fungi. Med Mycol. 2008 Dec 1;46(8):749–72.

873 63. Mattoon ER, Cordero RJB, Casadevall A. Fungal Melanins and Applications in Healthcare,
874 Bioremediation and Industry. J Fungi (Basel). 2021 Jun 18;7(6):488.

875 64. Nosanchuk JD, Casadevall A. Impact of melanin on microbial virulence and clinical resistance to
876 antimicrobial compounds. Antimicrob Agents Chemother. 2006 Nov;50(11):3519–28.

877 65. Zamith-Miranda D, Heyman HM, Cleare LG, Couvillion SP, Clair GC, Bredeweg EL, et al. Multi-omics
878 Signature of Candida auris, an Emerging and Multidrug-Resistant Pathogen. mSystems [Internet].
879 2019 Jun 11 [cited 2022 Jan 19]; Available from:
880 https://journals.asm.org/doi/abs/10.1128/mSystems.00257-19

881 66. Schindelin J, Arganda-Carreras I, Frise E, Kaynig V, Longair M, Pietzsch T, et al. Fiji: an open-source
882 platform for biological-image analysis. Nature Methods. 2012 Jul;9(7):676–82.

883 67. Chatterjee S, Prados-Rosales R, Itin B, Casadevall A, Stark RE. Solid-state NMR Reveals the
884 Carbon-based Molecular Architecture of Cryptococcus neoformans Fungal Eumelanins in the Cell
885 Wall. J Biol Chem. 2015 May 29;290(22):13779–90.

886 68. Vij R, Danchik C, Crawford C, Dragotakes Q, Casadevall A. Variation in Cell Surface Hydrophobicity
887 among Cryptococcus neoformans Strains Influences Interactions with Amoebas. mSphere
888 [Internet]. 2020 Apr 29 [cited 2020 Sep 21];5(2). Available from:
889 https://msphere.asm.org/content/5/2/e00310-20

890

891
892 **Figure Legends:**
893
894 ***Figure 1. Effect of Temperature on Melanization.*** Melanization variably occurs in *C. auris* strains. This
895 melanization can be quantified (A). Melanization occurs less at 30˚C (B) than at 37˚C (C) particularly for
896 the melanizing strains CDC 388, CDC 390, and MMC1. Experiments performed in biological replicates.
897 Panels (B) and (C) are representative images. (D-F) Electronic paramagnetic resonance (EPR) of
898 melanin isolated from *Cryptococcus neoformans* (D), non-melanizing *C. auris* strains (E) and melanizing
899 *C. auris* strains (F) grown in minimal media with L-DOPA. Error bars represent standard deviation from
900 three independent experiments.

901 ***Figure 2. Cell density and time course.*** *C. auris* yeast cells were incubated at increasing cell densities
902 in minimal media in the presence, or absence, of L-DOPA. Melanin formation was monitored through the
903 course of 13 days and quantified using ImageJ. The graphs show means and standard deviation from 3
904 independent experiments.

905 ***Figure 3. Melanization by Substrate.*** **(A)** *C. auris* melanizing strains use catecholamines such as L-
906 DOPA, D-DOPA, Methyl-DOPA, dopamine, epinephrine, and norepinephrine as substrates for
907 melanization. Overall, there are few differences between the melanizing strains' abilities to oxidize these
908 substrates. **(B)** The color of the pigments formed were typically brown-black, with the exception of the
909 orange produced with epinephrine. Red dotted line represents the baseline mean gray value of the
910 background. Values above the line (closer to 0) signify wells darker than the background. **(C)** Strains of *C.*
911 *auris,* CDC 381, 387, and 388 do not have laccase activity when grown with the laccase-specific
912 substrate ABTS, while the positive control – H99 strain of *Cryptococcus neoformans* – does have
913 laccase activity, as indicated by the blue color formed in culture. Data represents biological triplicate, with
914 Panel **(B,C)** showing a representative image of the melanized cultures. Abbreviations: L-Tyrosine (TYR),
915 Methyl-DOPA (M-DOPA), dopamine (DA), epinephrine (EPI), norepinephrine (NOR), Brain mixture
916 (BRAIN), homogentisic acid (HGA), 4-hydroxyphenylpyruvic acid (4-HPP), Caspofungin (CASPO). Error
917 bars indicate standard deviation.

918 ***Figure 2. Melanization primarily occurs extracellularly in C. auris*****. (A-B)** The supernatant of
919 melanized cultures have darker supernatants than their non-melanized counterparts, particularly the
920 supernatant from the CDC 388 strain. **(C)** When grown on solid agar, all melanizing strains have a dark
921 halo surrounding their colony, with darker color around strong melanizing strains. The colonies of the
922 strains themselves are notably white. **(D)** The cell-free supernatant from CDC 387 and CDC 388
923 (melanin-capable strains) have the ability to melanize, indicating a melanization factor is present. **(E-F)**
924 Cultures grown with L-DOPA have melanin particles in the supernatant that can be collected and
925 visualized via electron microscopy. The strongly melanizing CDC 387 strain has the largest population of
926 these particles, the moderate melanizing strains CDC 388 and MMC1 have moderately sized population
927 of these particles, and the weak melanizing strain CDC 381 has the smallest population. All experiments
928 done in biological triplicate. Panels **(A), (C)** and **(F)** are representative images. Scale Bar indicates 500
929 nm. Error bars indicate standard deviation.

930 ***Figure 5. Melanin is Primarily Deposited on the Cell Wall Surface.*** **(A)** Light Microscopy shows that
931 the 387, 388, and MMC1 cells have darker color when grown in minimal media with L-DOPA, while there
932 is little color change in the CDC 381 cell color. Some of the pigmented cells have dark pigmentation
933 within the cell. CDC 387 in particular appears to have large pigmented extracellular structures. Scale bars
934 represent 10 μm. Images representative of three biological replicates. **(B)** Transmission electron

935 microscopy shows electron dense particles on the outside of only the 387, 388, and MMC1 cells grown in
936 the presence of L-DOPA, which is indicative of melanin pigment. These dark particles are found on the
937 external cell wall and in the extracellular space, and are especially visible in the CDC 387 and MMC1
938 micrographs. Scale bars represent 500 nm. **(C)** Similar external granule structures on the surface of CDC
939 387, 388, and MMC1 cells grown with L-DOPA can be seen in SEM micrographs. Scale bars represent 5
940 μm.

941 ***Figure 6. Extracellular Melanin Adheres to β-glucans.*** **(A-C)** Adding non-melanized cells to the
942 melanized supernatant from its corresponding strain resulted in pigmented cells after 3 hours of
943 incubation. **(D)** The melanized supernatant from the CDC 388 strain causes the non-melanizing CDC 381
944 strain to become pigmented. Adding the building block for chitin, GlcNAc, to the CDC 387 (**E)** and CDC
945 388 (**F)** resulted in increased supernatant melanization, blocking chitin synthesis with CFW resulted in
946 less melanin in supernatant but also caused melanin coated CFW crystals on the fungal surface. Blocking
947 β-Glucan synthesis with caspofungin resulted in increased supernatant melanization in both strains. **(G-H)**
948 Electron microscopy revealed no major differences in melanin adherence to the cell wall in either the
949 CDC 387 **(G)** and CDC 388 **(H)** strains treated with GlcNAc. There were clear electron-dense crystal
950 structures on the cell walls of CFW conditions, and the caspofungin-treated conditions had little to no
951 melanin on the cell surface. While caspofungin-treated cells grew in culture, they look atypical in TEM
952 with a condensed cytoplasm. All scale bars represent 500 nm. **(I,J)** There is no association between the
953 hydrophobicity of a *C. auris* strain and its ability to melanize. **(K)** Although, the melanization of certain
954 strains, namely CDC 387, results in a significant reduction of CSH compared to its non-melanized control.
955 No statistically reduction that happens in CDC 381, 388, or MMC1 strains. All experiments are
956 representative of three biological replicates. Statistical differences tested with a Two-Way ANOVA with
957 multiple comparisons using Prism GraphPad, with $p<0.0001$ = ****. Error bars indicate standard deviation.

958 ***Figure 7. C. auris Melanization Factor is Resistant to Denaturing Conditions. (*****A)** Heating the
959 supernatant to 100˚C slightly reduces the melanizing ability of the supernatant but does not completely
960 abolish melanizing ability of the supernatant nor the precipitate that forms following boiling (inset). Adding
961 proteinase K (**B**) or Trypsin (**C**) does not reduce the melanizing ability of the supernatant. **(D)** Images of
962 the oxidation after 72 h within the samples treated with proteinase K and trypsin (E) Similarly, 33%
963 methanol and 1% SDS did not reduce melanization activity, while 6M urea uniformly enhanced DOPA
964 oxidation in all groups. **(F)** Filtration through a 3 kDa filter indicates that the melanizing factor is smaller
965 than 3 kDa. **(G)** The melanizing factor is not protected from proteolytic degradation by being shielded
966 within extracellular vesicles (EV), as addition of detergent to disturb EVs does not render the melanization
967 factor more suscept to proteolytic degradation. Error bars indicate standard deviation.

968 ***Figure 3. Supernatant pH Correlates to Melanization Ability. (*****A)** The pH of the supernatant from the
969 *C. auris* cultures corresponds to the ability of that strain to melanize, with two distinct clusters that
970 correspond to melanizing versus non-melanizing strains. **(B)** The correlation between pH and
971 melanization from the *C. auris* strains corresponds to a similar increase in autoxidation of L-DOPA in the
972 same range of pH. **(C)** Reducing the pH of the supernatants to 5.5 abolished melanization ability in the
973 CDC 387 and 388 strains, while raising the pH of the supernatants to 7 enhanced melanization in all the
974 supernatants, including CDC 381. **(D)** Images of the L-DOPA oxidation in the supernatant following pH
975 alteration. **(E,F)** *C. auris* strains that melanize are associated with increased ammonia concentration in
976 the supernatant, with a concentration of approximately 16 ppm, while non-melanizing strains have an
977 ammonia concentration between 8 and 5 ppm. **(G)** Aggregates from pH 7 melanized cell-free supernatant
978 from CDC 387 and CDC 388 look similar to those produced in cultures (Figure 4F), whereas the pigment

979 collected from the pH 7 minimal media looks more amorphous and lacks structure. The Scale Bar
980 represents 500 nm. Error bars indicate standard deviation.

981 **Figure 9. Melanin from *C. auris* during interaction with the host**. (**A**) Melanized and control yeast cells
982 were incubated with, or without, hydrogen peroxide (H_2O_2) 5 mM for 3 hours at 37° C. Yeast viability was
983 addressed by CFU counting and values of H_2O_2-treated *C. auris* were expressed as a percentage of cells
984 in the absence of H_2O_2. Each symbol in the graph represents one experiment performed in triplicates.
985 Data was treated by One-way ANOVA followed by Sidak's multiple comparison test. (**B**) Bone marrow-
986 derived macrophages (BMDM) were challenged with melanized or control *C. auris* yeast cells for 2 or 24
987 hours. After macrophage lysis, fungal viability was addressed by CFU counting. The killing percentage
988 was expressed as the amount of viable yeast in the presence of macrophages, divided by the amount of
989 yeast in the absence of macrophages for each strain and condition. Each symbol represents one
990 experiment performed in triplicates. (**C**) Melanized and control *C. auris* yeast cells were inoculated into
991 the haemocoel of *G. mellonella* larvae (n = 10/group). The number of living larvae was monitored for 7
992 days after inoculation.
993
994 ***Figure 10. Proposed Model for Candida auris Melanization.*** *C. auris* from Clades I and IV can
995 neutralize the pH of their surrounding environment by secreting either ammonia, an alkalinizing enzyme,
996 or some other pH modulator. The neutralized pH encourages oxidation of catecholamines present, which
997 begin to form a pigment. The oxidized catecholamines may aggregate on secreted proteins,
998 polysaccharides, or lipids to form melanin granules. These melanin granules are deposited on the surface
999 of the fungi. In cases of high degrees of melanization, nearly all the extracellular melanin ends up
1000 adhering to the surface of the fungus, leaving a relatively light-colored supernatant.

1001 ***Supplementary Figure 1. Interactions of Calcofluor White and Melanin. (***A) Melanizing *C. auris*
1002 strains (CDC 387) grown with L-DOPA and Calcofluor white (CFW) have visible crystal formation under
1003 light microscopy. These crystals are dark in color, suggesting the presence of melanin or polymerized L-
1004 DOPA, and they are fluorescent under a 405 nm wavelength laser, indicating they also contain CFW. (B)
1005 These crystals can also be seen under transmission electron microscopy. (C) Adding L-DOPA and CFW
1006 to non-melanized cell-free supernatant resulted in the formation of black crystals, which under the
1007 fluorescent microscope have signal, indicating that the crystals are a combination of both CFW and
1008 melanin/autopolymerized L-DOPA. (D) Additionally, when CFW is added to supernatant, the crystals that
1009 form in CDC 381 strain are large and settle quickly, leaving few crystals in suspension, whereas CDC 387
1010 and 388 form smaller crystals that do not settle rapidly and remain in the suspension. Inset is an image of
1011 the falcon tube containing the supernatant with CFW, and micrographs show a sample taken from the
1012 non-settled suspension. (E) Pseudohyphal morphology seen in the melanized CDC 388 culture treated
1013 with 50% MIC caspofungin for 1 week. Scale bars in A, C, D, and E represent 10 μm, and scale bars in B
1014 represent 500 nm.
1015
1016 ***Supplementary Figure 2. Melanization activity is not associated with Extracellular Vesicles.***
1017 Following ultracentrifugation of the *C. auris*-conditioned media, there is equal melanization activity in both
1018 the supernatant and the pellet (containing extracellular vesicles) resuspended in 200 μl of supernatant,
1019 which represents a ~200x concentration.
1020
1021 ***Supplementary Table 1.*** **List of laccase homologues in *C. auris* from FungiDB**
1022
1023 ***Supplementary Table 2.*** **List of tyrosinase homologues in *C. auris* from FungiDB**

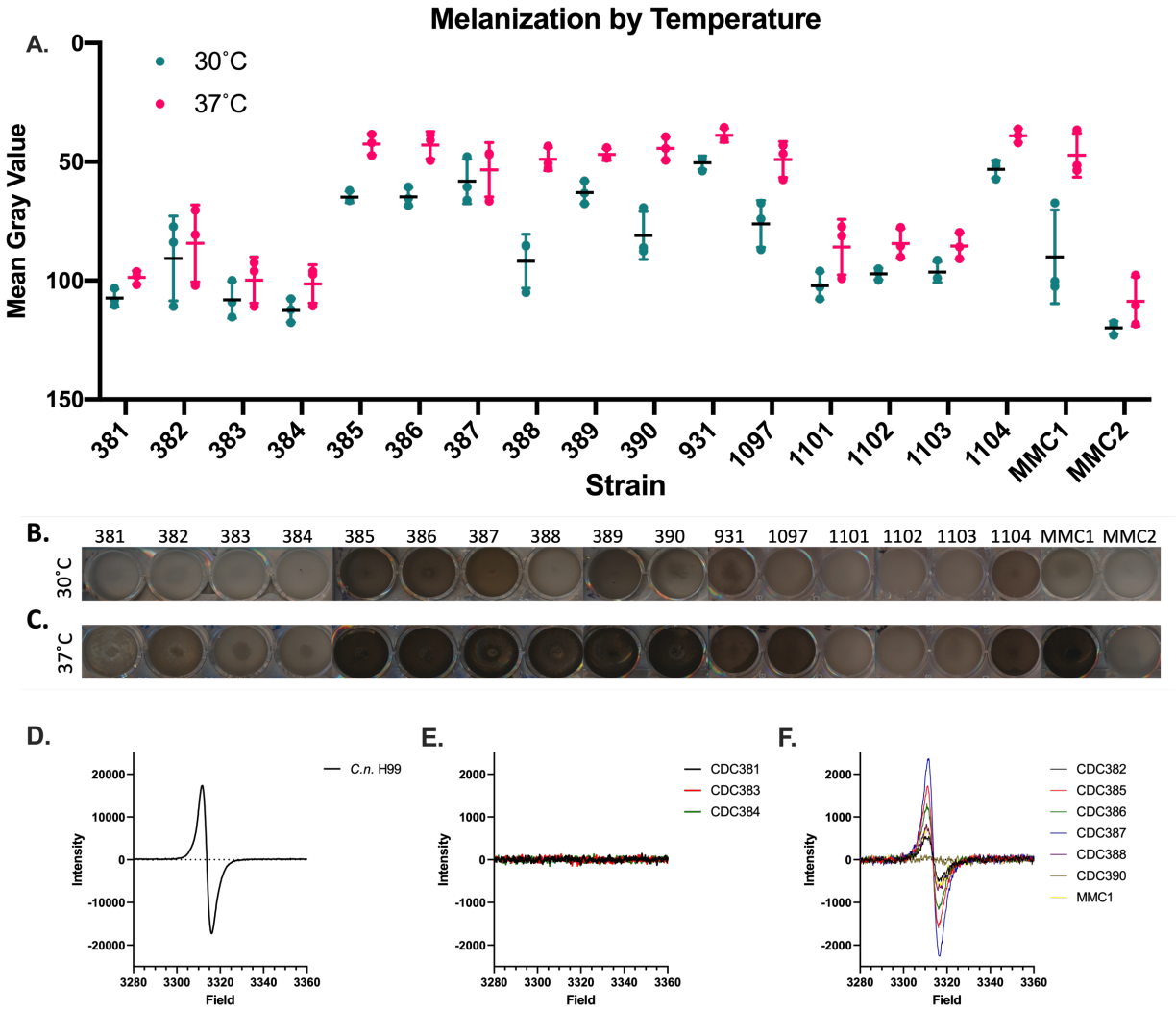

Figure 1. Effect of Temperature on Melanization. Melanization occurs in only some of the *C. auris* strains. This melanization can be quantified (A). Melanization occurs less at 30˚C (B) than at 37˚C (C) particularly for the melanizing strains CDC 388, CDC 390, and MMC1. Experiments performed in biological replicates. Panels (B) and (C) are representative images. (D-F) Electronic paramagnetic resonance (EPR) of melanin isolated from *Cryptococcus neoformans* (D), non-melanizing *C. auris* strains (E) and melanizing *C. auris* strains (F) grown in minimal media with L-DOPA. Error bars represent standard deviation from three independent experiments.

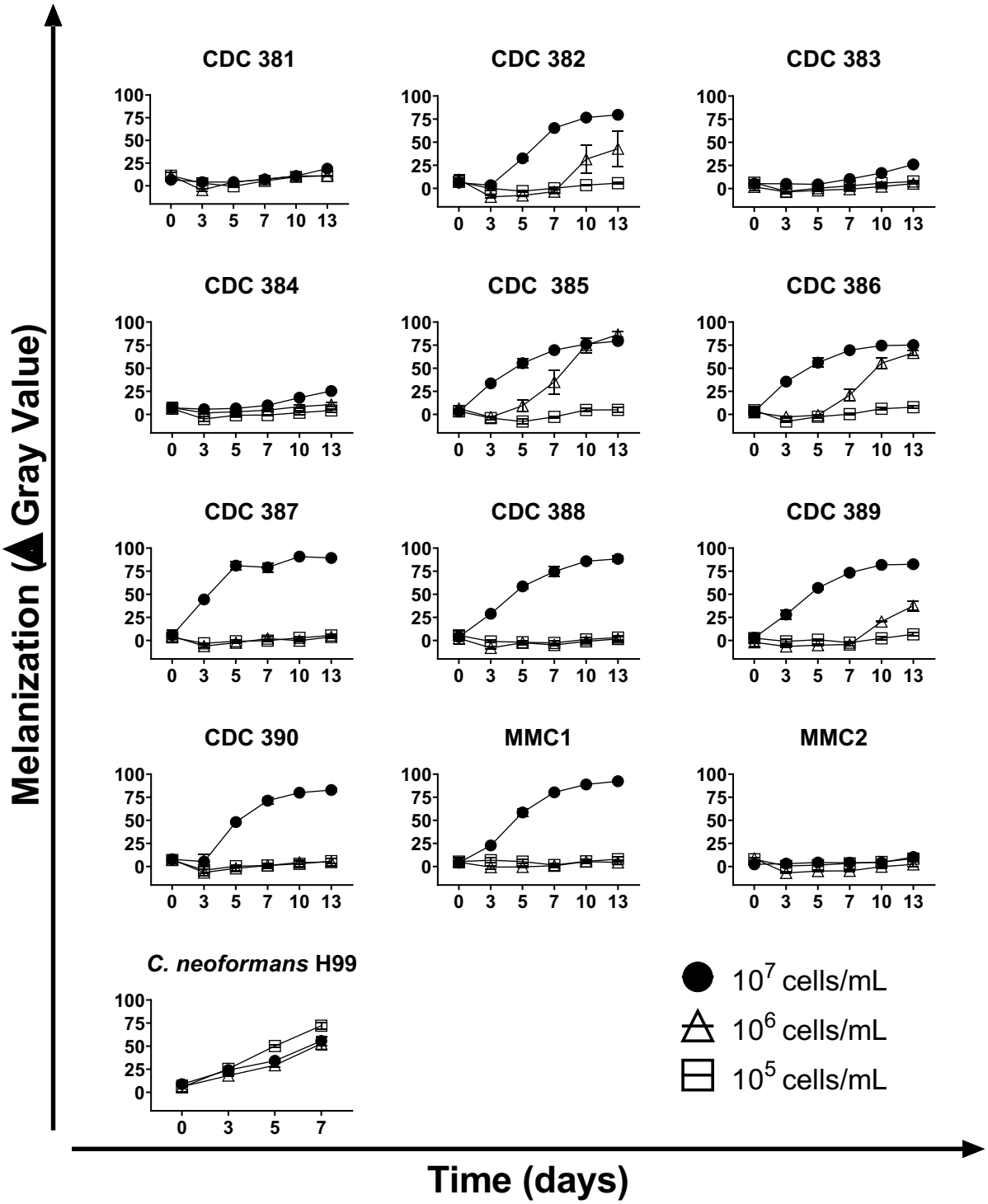

Figure 2. Cell density and time course. *C. auris* yeast cells were incubated at increasing cell densities in minimal media in the presence, or absence, of L-DOPA. Melanin formation was monitored through the course of 13 days and quantified using ImageJ. The graphs show means and standard deviation from 3 independent experiments.

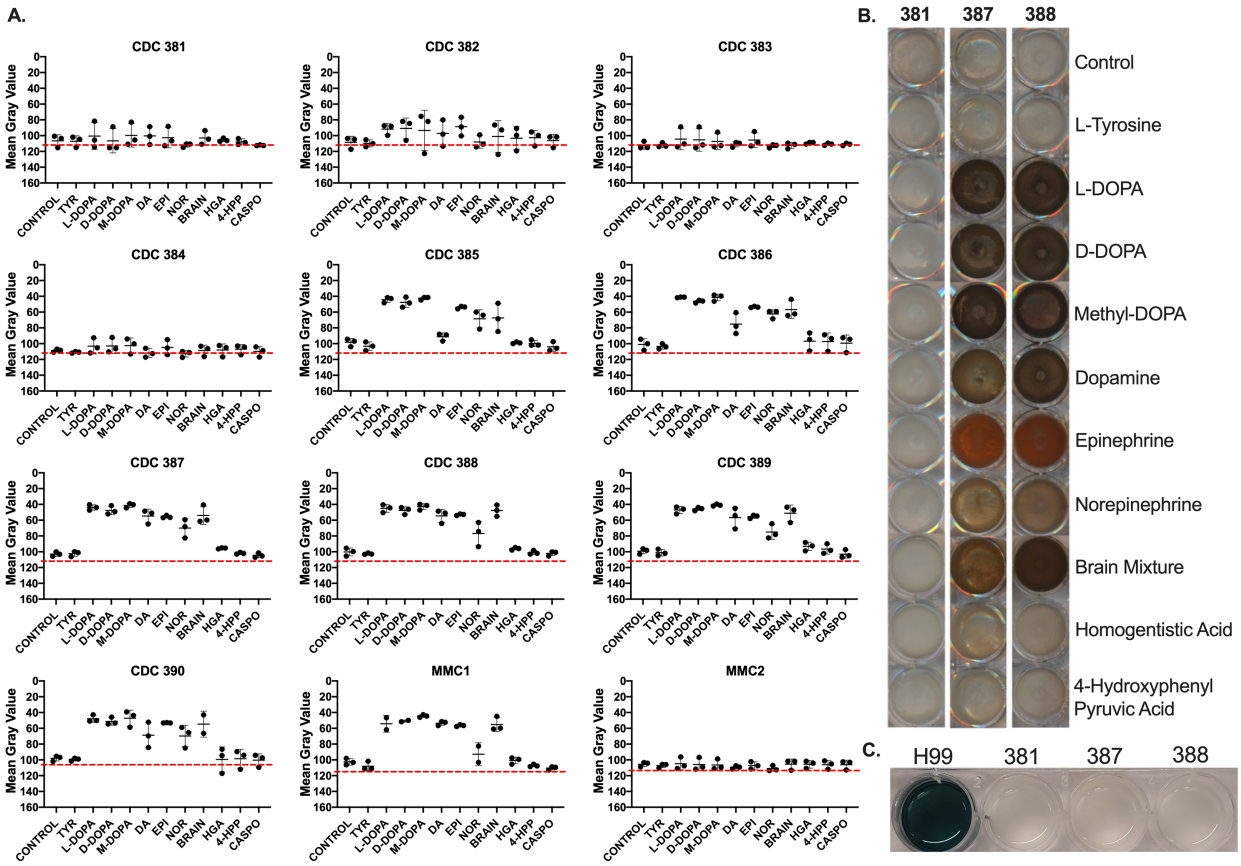

Figure 3. Melanization by Substrate. **(A)** *C. auris* melanizing strains use catecholamines such as L-DOPA, D-DOPA, Methyl-DOPA, dopamine, epinephrine, and norepinephrine as substrates for melanization. Overall, there are few differences between the melanizing strains' abilities to oxidize these substrates. **(B)** The color of the pigments formed were typically brown-black, with the exception of the orange produced with epinephrine. Red dotted line represents the baseline mean gray value of the background. Values above the line (closer to 0) signify wells darker than the background. (**C)** Strains of *C. auris,* CDC 381, 387, and 388 do not have laccase activity when grown with the laccase-specific substrate ABTS, while the positive control – H99 strain of *Cryptococcus neoformans* – does have laccase activity, as indicated by the blue color formed in culture. Data represents biological triplicate, with Panel **(B,C)** showing a representative image of the melanized cultures. Abbreviations: L-Tyrosine (TYR), Methyl-DOPA (M-DOPA), dopamine (DA), epinephrine (EPI), norepinephrine (NOR), Brain mixture (BRAIN), homogentisic acid (HGA), 4-hydroxyphenylpyruvic acid (4-HPP), Caspofungin (CASPO). Error bars indicate standard deviation.

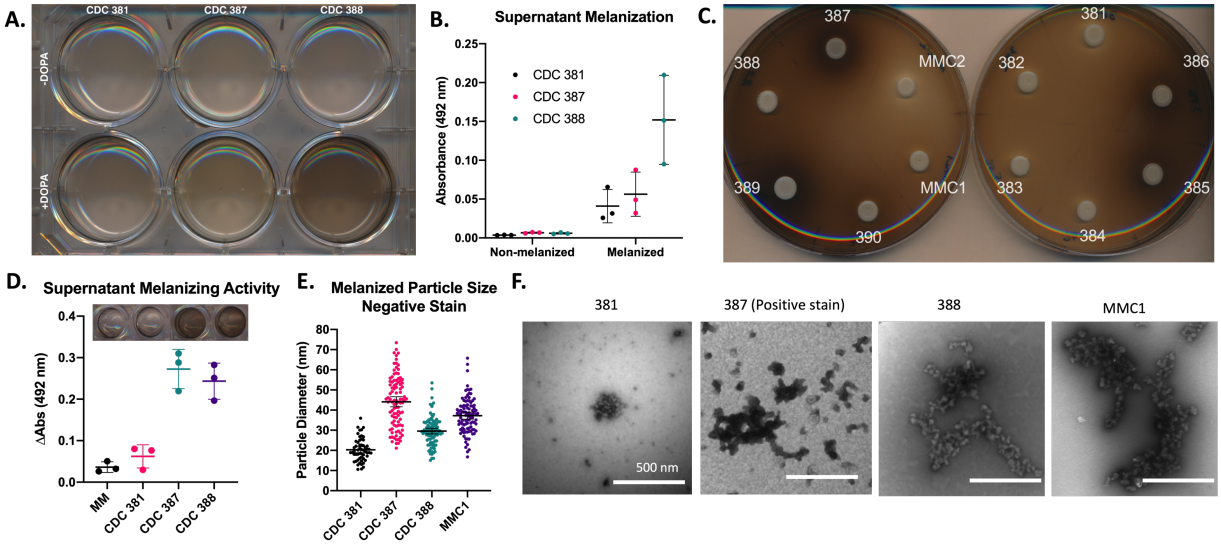

***Figure 2. Melanization primarily occurs extracellularly in C. auris*. (A-B)** The supernatant of melanized cultures have darker supernatants than their non-melanized counterparts, particularly the supernatant from the CDC 388 strain. **(C)** When grown on solid agar, all melanizing strains have a dark halo surrounding their colony, with darker color around strong melanizing strains. The colonies of the strains themselves are notably white. **(D)** The cell-free supernatant from CDC 387 and CDC 388 (melanin-capable strains) have the ability to melanize, indicating a melanization factor is present. **(E-F)** Cultures grown with L-DOPA have melanin particles in the supernatant that can be collected and visualized via electron microscopy. The strongly melanizing CDC 387 strain has the largest population of these particles, the moderate melanizing strains CDC 388 and MMC1 have moderately sized population of these particles, and the weak melanizing strain CDC 381 has the smallest population. All experiments done in biological triplicate. Panels **(A), (C)** and **(F)** are representative images. Scale Bar indicates 500 nm. Error bars indicate standard deviation.

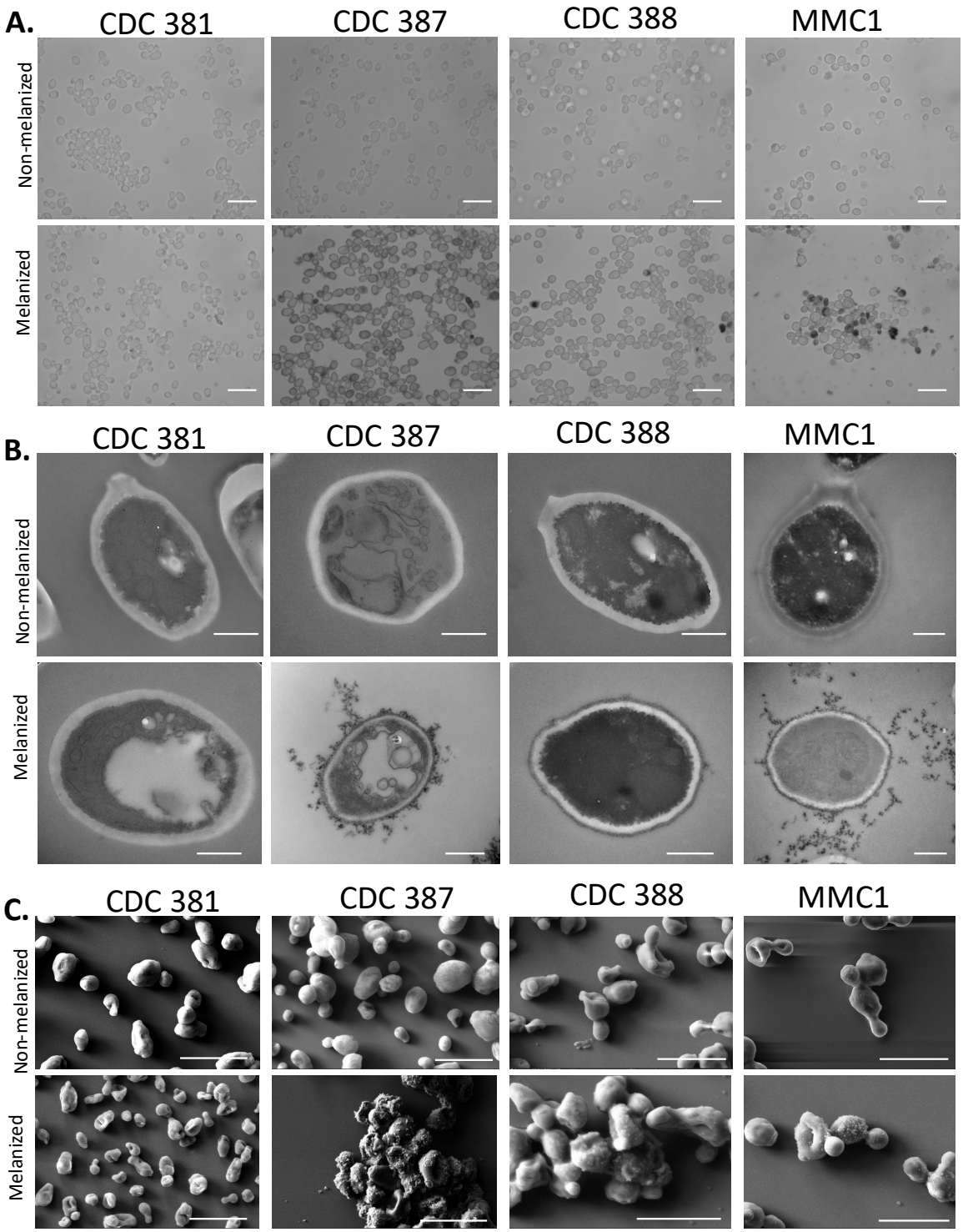

Figure 5. Melanin is Primarily Deposited on the Cell Wall Surface. **(A)** Light Microscopy shows that the 387, 388, and MMC1 cells have darker color when grown in minimal media with L-DOPA, while there is little color change in the CDC 381 cell color. Some of the pigmented cells have dark pigmentation within the cell. CDC 387 in particular appears to have large pigmented extracellular structures. Scale bars represent 10 µm. Images representative of three biological replicates. **(B)** Transmission electron microscopy shows electron dense particles on the outside of only the 387, 388, and MMC1 cells grown in the presence of L-DOPA, which is indicative of melanin pigment. These dark particles are found on the external cell wall and in the extracellular space, and are especially visible in the CDC 387 and MMC1 micrographs. Scale bars represent 500 nm. **(C)** Similar external granule structures on the surface of CDC 387, 388, and MMC1 cells grown with L-DOPA can be seen in scanning electron micrographs. Scale bars represent 5 µm.

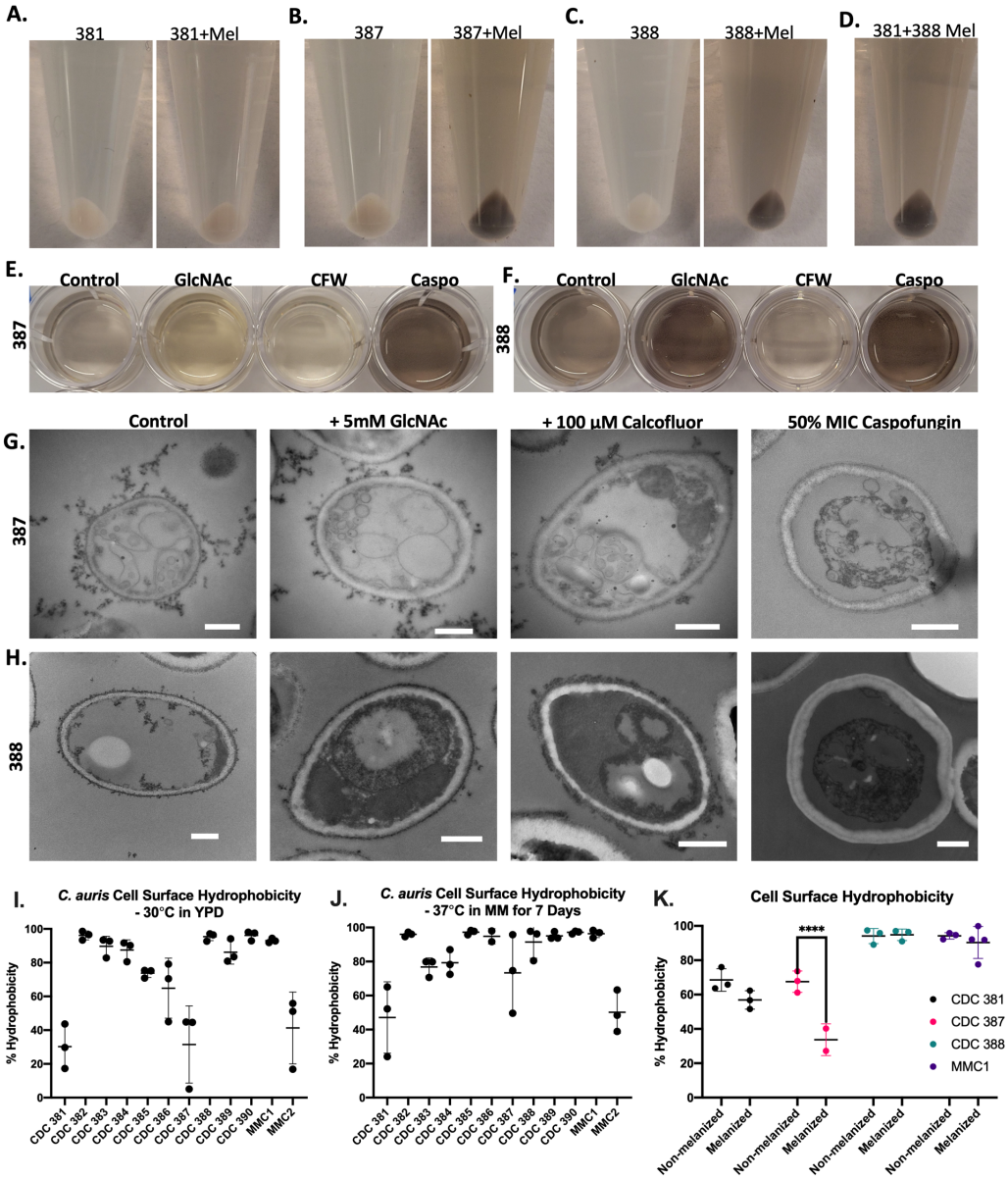

Figure 6. Extracellular Melanin Adheres to β-glucans. **(A-C)** Adding non-melanized cells to the melanized supernatant from its corresponding strain resulted in pigmented cells after 3 hours of incubation. **(D)** The melanized supernatant from the CDC 388 strain causes the non-melanizing CDC 381 strain to become pigmented. Adding the building block for chitin, GlcNAc, to the CDC 387 (**E)** and CDC 388 (**F)** resulted in increased supernatant melanization, blocking chitin synthesis with CFW resulted in less melanin in supernatant but also caused melanin-coated CFW crystals on the fungal surface. Blocking beta-Glucan synthesis with caspofungin resulted in increased supernatant melanization in both strains. **(G-H)** Electron microscopy revealed no major differences in melanin adherence to the cell wall in either the CDC 387 **(G)** and CDC 388 **(H)** strains treated with GlcNAc. There were clear electron-dense crystal structures on the cell walls of CFW conditions, and the caspofungin-treated conditions had little to no melanin on the cell surface. While caspofungin-treated cells grew in culture, they look atypical in TEM with a condensed cytoplasm. All scale bars represent 500 nm. **(I,J)** There is no association between the hydrophobicity of a *C. auris* strain and its ability to melanize. **(K)** Although, the melanization of certain strains, namely CDC 387, results in a significant reduction of CSH compared to its non-melanized control. No statistically reduction reduction that happens in CDC 381, 388, or MMC1 strains. All experiments are representative of three biological replicates. Statistical differences tested with a Two-Way ANOVA with multiple comparisons using Prism GraphPad, with $p<0.0001$ = ****. Error bars indicate standard deviation.

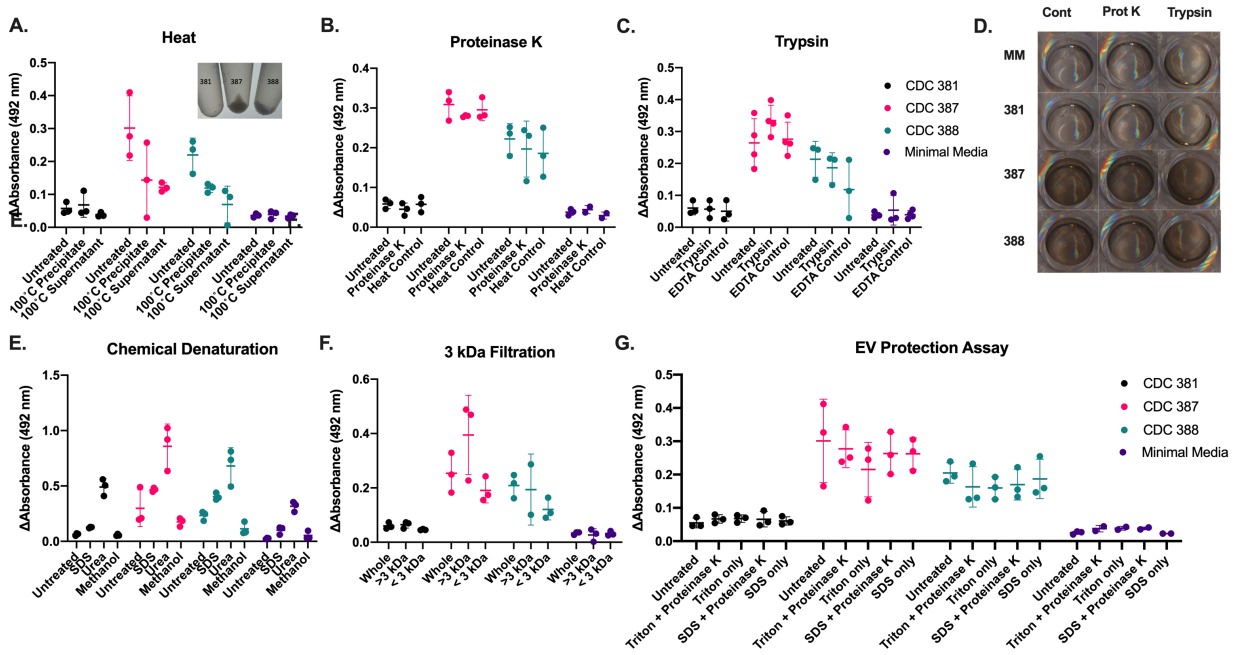

Figure 7. C. auris Melanization Factor is Resistant to Denaturing Conditions. (*A*) Heating the supernatant to 100˚C slightly reduces the melanizing ability of the supernatant but does not completely abolish melanizing ability of the supernatant nor the precipitate that forms following boiling (inset). Adding proteinase K (**B**) or Trypsin (**C**) does not reduce the melanizing ability of the supernatant. **(D)** Images of the oxidation after 72 h within the samples treated with proteinase K and trypsin (E) Similarly, 33% methanol and 1% SDS did not reduce melanization activity, while 6M urea uniformly enhanced DOPA oxidation in all groups. **(F)** Filtration through a 3 kDa filter indicates that the melanizing factor is smaller than 3 kDa. **(G)** The melanizing factor is not protected from proteolytic degradation by being shielded within extracellular vesicles (EV), as addition of detergent to disturb EVs does not render the melanization factor more suscept to proteolytic degradation. Error bars indicate standard deviation.

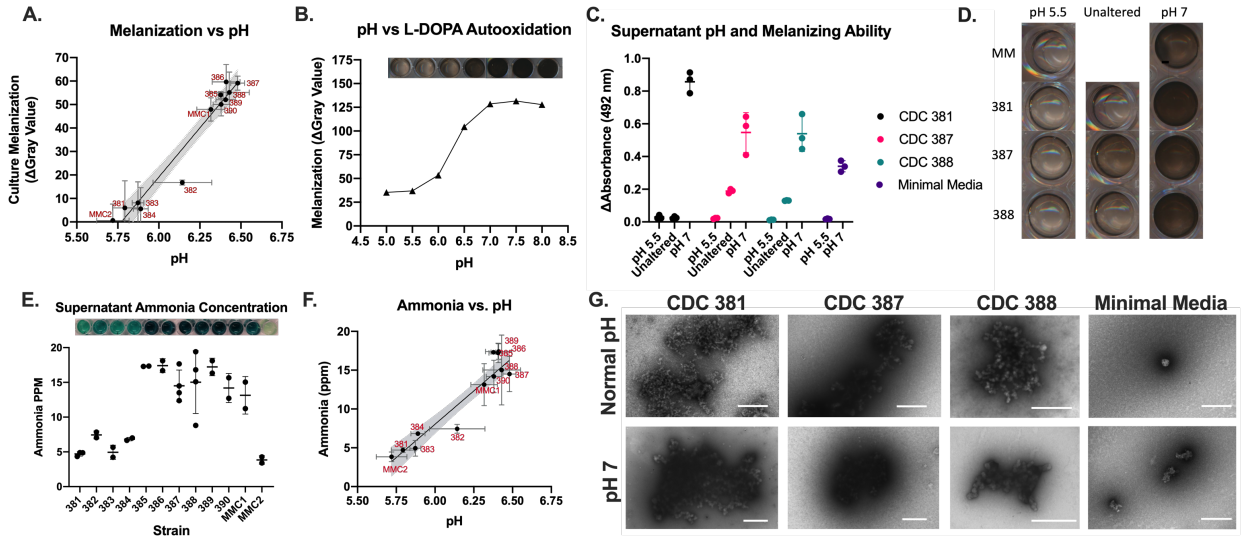

Figure 3. Supernatant pH Correlates to Melanization Ability. (*A*) The pH of the supernatant from the *C. auris* cultures corresponds to the ability of that strain to melanize, with two distinct clusters that correspond to melanizing versus non-melanizing strains. **(B)** The correlation between pH and melanization from the *C. auris* strains corresponds to a similar increase in autoxidation of L-DOPA in the same range of pH. **(C)** Reducing the pH of the supernatants to 5.5 abolished melanization ability in the CDC 387 and 388 strains, while raising the pH of the supernatants to 7 enhanced melanization in all the supernatants, including CDC 381. **(D)** Images of the L-DOPA oxidation in the supernatant following pH alteration. **(E,F)** *C. auris* strains that melanize are associated with increased ammonia concentration in the supernatant, with a concentration of approximately 16 ppm, while non-melanizing strains have an ammonia concentration between 8 and 5 ppm. **(G)** Aggregates from pH 7 melanized cell-free supernatant from CDC 387 and CDC 388 look similar to those produced in cultures (Figure 4F), whereas the pigment collected from the pH 7 minimal media looks more amorphous and lacks structure. The Scale Bar represents 500 nm. Error bars indicate standard deviation.

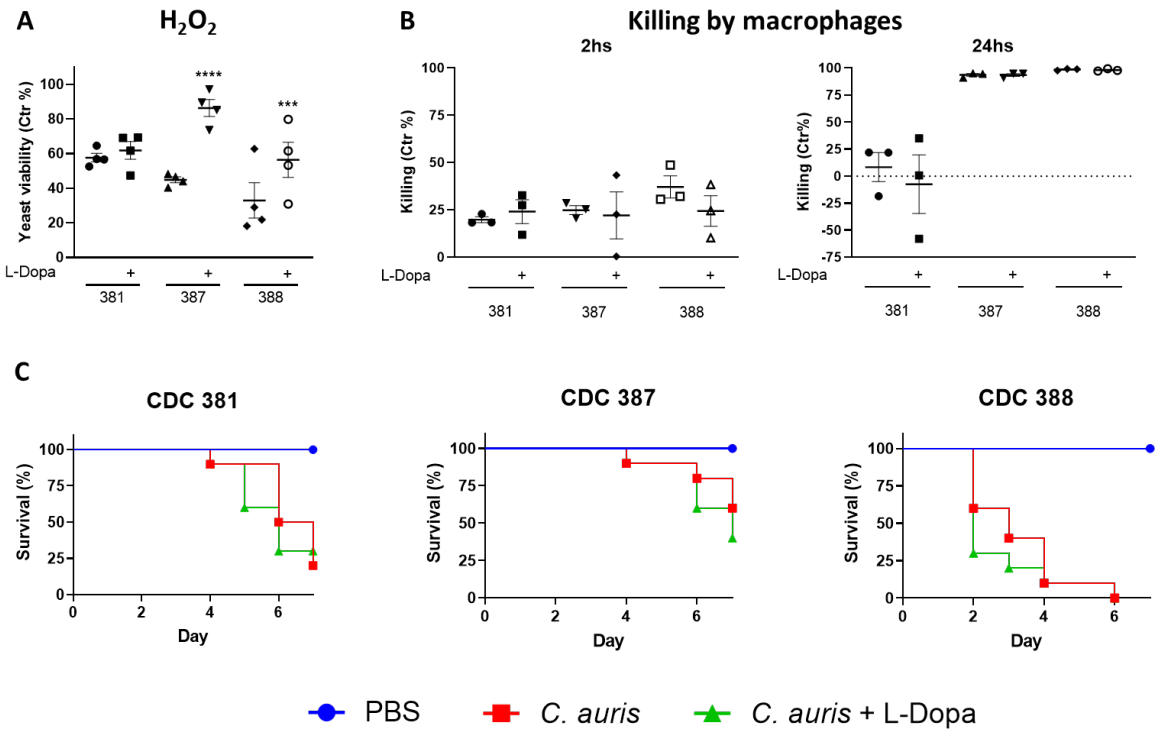

Figure 9. Melanin from *C. auris* during interaction with the host. (**A**) Melanized and control yeast cells were incubated with, or without, hydrogen peroxide (H_2O_2) 5 mM for 3 hours at 37° C. Yeast viability was addressed by CFU counting and values of H_2O_2-treated *C. auris* were expressed as a percentage of cells in the absence of H_2O_2. Each symbol in the graph represents one experiment performed in triplicates. Data was treated by One-way ANOVA followed by Sidak's multiple comparison test. (**B**) Bone marrow-derived macrophages (BMDM) were challenged with melanized or control *C. auris* yeast cells for 2 or 24 hours. After macrophage lysis, fungal viability was addressed by CFU counting. The killing percentage was expressed as the amount of viable yeast in the presence of macrophages, divided by the amount of yeast in the absence of macrophages for each strain and condition. Each symbol represents one experiment performed in triplicates. (**C**) Melanized and control *C. auris* yeast cells were inoculated into the haemocoel of *G. mellonella* larvae (n = 10/group). The number of living larvae was monitored for 7 days after inoculation.

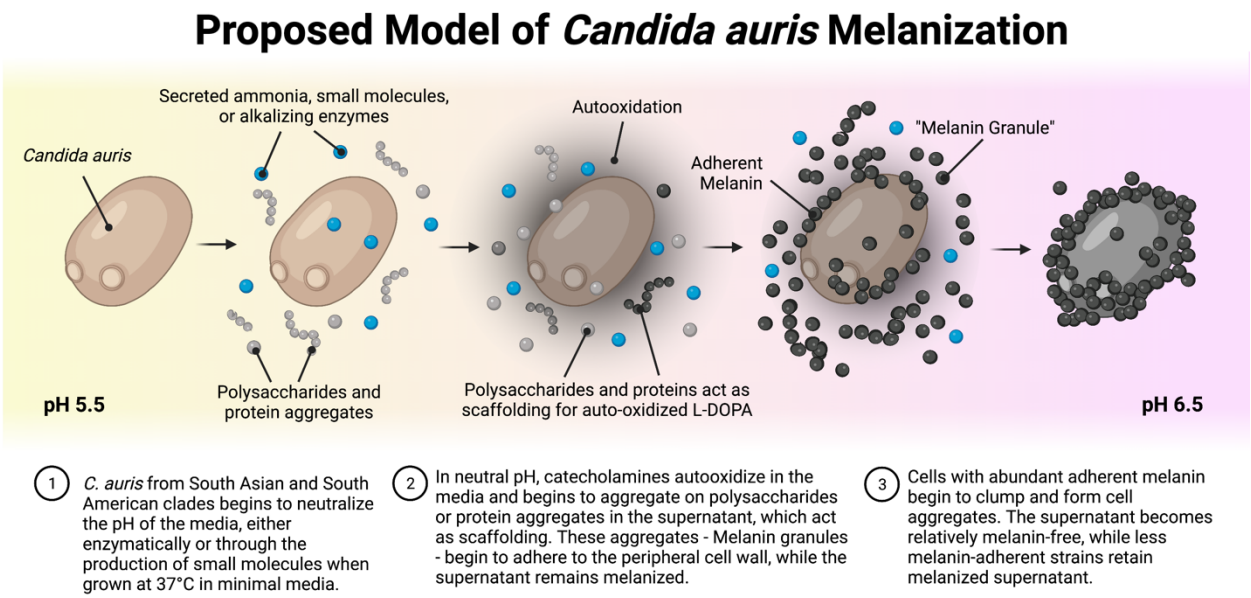

Figure 10. Proposed Model for Candida auris Melanization. *C. auris* from Clades I and IV are able to neutralize the pH of their surrounding environment by secreting either ammonia, an alkalinizing enzyme, or some other pH modulator. The neutralized pH encourages oxidation of catecholamines present, which begin to form a pigment. The oxidized catecholamines may aggregate on secreted proteins, polysaccharides, or lipids to form melanin granules. These melanin granules are deposited on the surface of the fungi. In cases of high degrees of melanization, nearly all of the extracellular melanin ends up adhering to the surface of the fungus, leaving a relatively light-colored supernatant.

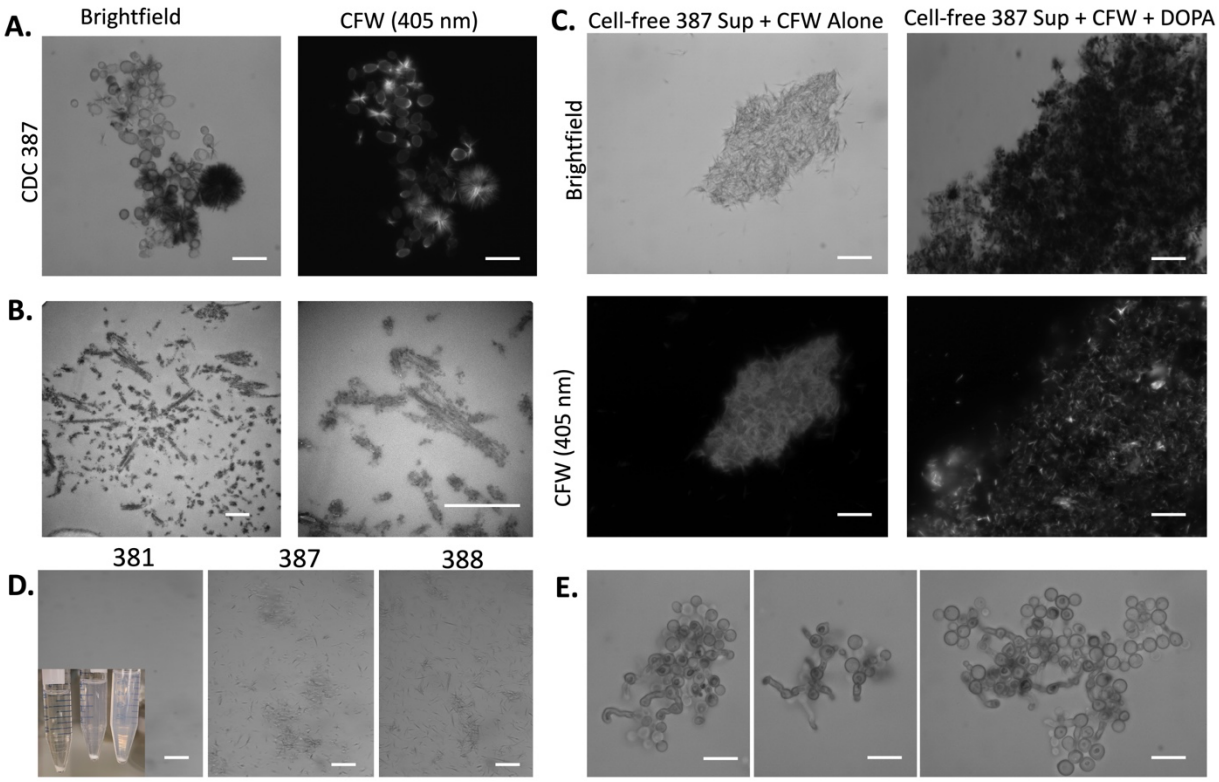

Supplementary Figure 1. Interactions of Calcofluor White and Melanin. (A)Melanizing *C. auris* strains (CDC 387) grown with L-DOPA and Calcofluor white (CFW) have visible crystal formation under light microscopy. These crystals are dark in color, suggesting the presence of melanin or polymerized L-DOPA, and they are fluorescent under a 405 nm wavelength laser, indicating they also contain CFW. (B) These crystals can also be seen under transmission electron microscopy. (C) Adding L-DOPA and CFW to non-melanized cell-free supernatant resulted in the formation of black crystals, which under the fluorescent microscope have signal, indicating that the crystals are a combination of both CFW and melanin/autopolymerized L-DOPA. (D) Additionally, when CFW is added to supernatant, the crystals that form in CDC 381 strain are large and settle quickly, leaving few crystals in suspension, whereas CDC 387 and 388 form smaller crystals that do not settle rapidly and remain in the suspension. Inset is an image of the falcon tube containing the supernatant with CFW, and micrographs show a sample taken from the non-settled suspension. Scale bars in A, C, D, and E represent 10 µm, and scale bars in B represent 500 nm.

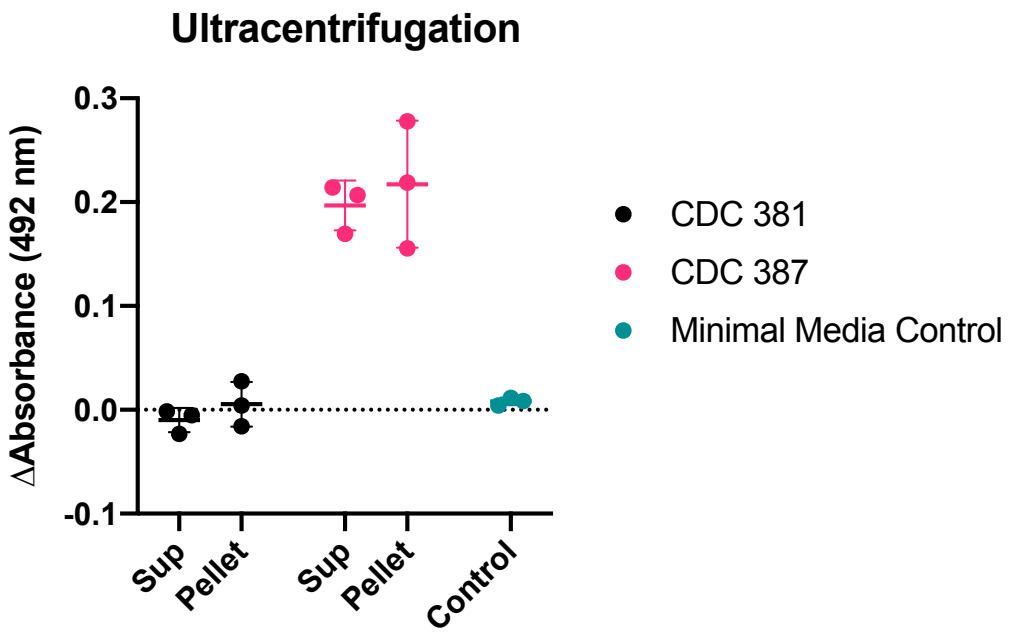

Supplementary Figure 2. Melanization activity is not associated with Extracellular Vesicles. Following ultracentrifugation of the *C. auris*-conditioned media, there is equal melanization activity in both the supernatant and the pellet (containing extracellular vesicles) resuspended in 200 µl of supernatant, which represents a ~200x concentration.

Organism	CDC Strain	Gene ID	Product Description	Ortholog Group	EC numbers from OrthoMCL	Computed GO Component IDs	Computed GO Components	Computed GO Function IDs	Computed GO Functions	Computed GO Process IDs	Computed GO Processes	Interpro ID	Interpro Description	PFam ID	PFam Description	Superfamily ID	Superfamily Description
Candida auris strain B11220	381	CJI96_0000827	hypothetical_protein	OG6_100257	1.10.3.2 (Laccase);1.10.3.3 (L-ascorbate oxidase);1.16.3.1 (Ferroxidase);1.7.2.1 (Nitrite reductase (NO-forming));2.7.-.- (Transferring phosphorus-containing groups.);3.2.1.- (Glycosidases, i.e. enzymes hydrolyzing O- and S-glycosyl compounds.);3.2.1.3 (Glucan 1,4-alpha-glucosidase);3.2.1.97 (Endo-a	GO:0016021	integral component of membrane	GO:0005507;GO:0016491	copper ion binding;oxidoreductase activity	GO:0006811;GO:0005072;GO:0055114	ion transport;iron ion homeostasis;obsolete oxidation-reduction process	IPR001117;IPR002355;IPR008972;IPR011706;IPR011707;IPR033138	Multicopper oxidase, type 1;Multicopper oxidase, copper-binding site;Cupredoxin;Multicopper oxidase, type 2;Multicopper oxidase, type 3;Multicopper oxidases, conserved site	PF00394;PF07731;PF07732	Multicopper oxidase, type 1;Multicopper oxidase, type 2;Multicopper oxidase, type 3	SSF49503	Cupredoxin
Candida auris strain B11220	381	CJI96_0001509	hypothetical_protein	OG6_100380	1.10.3.2 (Laccase)	GO:0016021	integral component of membrane	N/A	N/A	N/A	N/A	IPR007248	Mpv17/PMP22	PF04117	Mpv17/PMP22	N/A	N/A
Candida auris strain B11220	381	CJI96_0001510	hypothetical_protein	OG6_100380	1.10.3.2 (Laccase)	GO:0016021	integral component of membrane	N/A	N/A	N/A	N/A	IPR007248	Mpv17/PMP22	PF04117	Mpv17/PMP22	N/A	N/A
Candida auris strain B11220	381	CJI96_0003577	hypothetical_protein	OG6_100257	1.10.3.2 (Laccase);1.10.3.3 (L-ascorbate oxidase);1.16.3.1 (Ferroxidase);1.7.2.1 (Nitrite reductase (NO-forming));2.7.-.- (Transferring phosphorus-containing groups.);3.2.1.- (Glycosidases, i.e. enzymes hydrolyzing O- and S-glycosyl compounds.);3.2.1.3 (Glucan 1,4-alpha-glucosidase);3.2.1.97 (Endo-a	GO:0016021	integral component of membrane	GO:0005507;GO:0016491	copper ion binding;oxidoreductase activity	GO:0006811;GO:0005072;GO:0055114	ion transport;iron ion homeostasis;obsolete oxidation-reduction process	IPR001117;IPR002355;IPR008972;IPR011706;IPR011707;IPR033138	Multicopper oxidase, type 1;Multicopper oxidase, copper-binding site;Cupredoxin;Multicopper oxidase, type 2;Multicopper oxidase, type 3;Multicopper oxidases, conserved site	PF00394;PF07731;PF07732	Multicopper oxidase, type 1;Multicopper oxidase, type 2;Multicopper oxidase, type 3	SSF49503	Cupredoxin
Candida auris strain B11221	383	CJI97_000078	unspecified product	OG6_100380	1.10.3.2 (Laccase)	GO:0016021	integral component of membrane	N/A	N/A	N/A	N/A	IPR007248	Mpv17/PMP22	PF04117	Mpv17/PMP22	N/A	N/A
Candida auris strain B11221	383	CJI97_000519	unspecified product	OG6_100257	1.10.3.2 (Laccase);1.10.3.3 (L-ascorbate oxidase);1.16.3.1 (Ferroxidase);1.7.2.1 (Nitrite reductase (NO-forming));2.7.-.- (Transferring phosphorus-containing groups.);3.2.1.- (Glycosidases, i.e. enzymes hydrolyzing O- and S-glycosyl compounds.);3.2.1.3 (Glucan 1,4-alpha-glucosidase);3.2.1.97 (Endo-a	N/A	N/A	GO:0005507;GO:0016491	copper ion binding;oxidoreductase activity	GO:0006811;GO:0005072;GO:0055114	ion transport;iron ion homeostasis;obsolete oxidation-reduction process	IPR001117;IPR002355;IPR008972;IPR011706;IPR011707;IPR033138	Multicopper oxidase, type 1;Multicopper oxidase, copper-binding site;Cupredoxin;Multicopper oxidase, type 2;Multicopper oxidase, type 3;Multicopper oxidases, conserved site	PF00394;PF07731;PF07732	Multicopper oxidase, type 1;Multicopper oxidase, type 2;Multicopper oxidase, type 3	SSF49503	Cupredoxin
Candida auris strain B11221	383	CJI97_003068	unspecified product	OG6_100257	1.10.3.2 (Laccase);1.10.3.3 (L-ascorbate oxidase);1.16.3.1 (Ferroxidase);1.7.2.1 (Nitrite reductase (NO-forming));2.7.-.- (Transferring phosphorus-containing groups.);3.2.1.- (Glycosidases, i.e. enzymes hydrolyzing O- and S-glycosyl compounds.);3.2.1.3 (Glucan 1,4-alpha-glucosidase);3.2.1.97 (Endo-a	N/A	N/A	GO:0005507;GO:0016491	copper ion binding;oxidoreductase activity	GO:0055114	obsolete oxidation-reduction process	IPR001117;IPR002355;IPR008972;IPR011706;IPR011707;IPR033138	Multicopper oxidase, type 1;Multicopper oxidase, copper-binding site;Cupredoxin;Multicopper oxidase, type 2;Multicopper oxidase, type 3;Multicopper oxidases, conserved site	PF00394;PF07731;PF07732	Multicopper oxidase, type 1;Multicopper oxidase, type 2;Multicopper oxidase, type 3	SSF49503	Cupredoxin
Candida auris strain B11245	386	CJJ09_001108	unspecified product	OG6_100257	1.10.3.2 (Laccase);1.10.3.3 (L-ascorbate oxidase);1.16.3.1 (Ferroxidase);1.7.2.1 (Nitrite reductase (NO-forming));2.7.-.- (Transferring phosphorus-containing groups.);3.2.1.- (Glycosidases, i.e. enzymes hydrolyzing O- and S-glycosyl compounds.);3.2.1.3 (Glucan 1,4-alpha-glucosidase);3.2.1.97 (Endo-a	GO:0016021	integral component of membrane	GO:0005507;GO:0016491	copper ion binding;oxidoreductase activity	GO:0006811;GO:0005072;GO:0055114	ion transport;iron ion homeostasis;obsolete oxidation-reduction process	IPR001117;IPR002355;IPR008972;IPR011706;IPR011707;IPR033138	Multicopper oxidase, type 1;Multicopper oxidase, copper-binding site;Cupredoxin;Multicopper oxidase, type 2;Multicopper oxidase, type 3;Multicopper oxidases, conserved site	PF00394;PF07731;PF07732	Multicopper oxidase, type 1;Multicopper oxidase, type 2;Multicopper oxidase, type 3	SSF49503	Cupredoxin
Candida auris strain B11245	386	CJJ09_002041	unspecified product	OG6_100380	1.10.3.2 (Laccase)	GO:0016021	integral component of membrane	N/A	N/A	N/A	N/A	IPR007248	Mpv17/PMP22	PF04117	Mpv17/PMP22	N/A	N/A
Candida auris strain B11245	386	CJJ09_002042	unspecified product	OG6_100380	1.10.3.2 (Laccase)	GO:0016021	integral component of membrane	N/A	N/A	N/A	N/A	IPR007248	Mpv17/PMP22	PF04117	Mpv17/PMP22	N/A	N/A
Candida auris strain B11245	386	CJJ09_002483	unspecified product	OG6_100257	1.10.3.2 (Laccase);1.10.3.3 (L-ascorbate oxidase);1.16.3.1 (Ferroxidase);1.7.2.1 (Nitrite reductase (NO-forming));2.7.-.- (Transferring phosphorus-containing groups.);3.2.1.- (Glycosidases, i.e. enzymes hydrolyzing O- and S-glycosyl compounds.);3.2.1.3 (Glucan 1,4-alpha-glucosidase);3.2.1.97 (Endo-a	N/A	N/A	GO:0005507;GO:0016491	copper ion binding;oxidoreductase activity	GO:0006811;GO:0005072;GO:0055114	ion transport;iron ion homeostasis;obsolete oxidation-reduction process	IPR001117;IPR002355;IPR008972;IPR011706;IPR011707;IPR033138	Multicopper oxidase, type 1;Multicopper oxidase, copper-binding site;Cupredoxin;Multicopper oxidase, type 2;Multicopper oxidase, type 3;Multicopper oxidases, conserved site	PF00394;PF07731;PF07732	Multicopper oxidase, type 1;Multicopper oxidase, type 2;Multicopper oxidase, type 3	SSF49503	Cupredoxin
Candida auris strain B8441	387	B9J08_000072	hypothetical protein	OG6_100380	1.10.3.2 (Laccase)	GO:0016021	integral component of membrane	N/A	N/A	N/A	N/A	IPR007248	Mpv17/PMP22	PF04117	Mpv17/PMP22	N/A	N/A
Candida auris strain B8441	387	B9J08_000073	hypothetical protein	OG6_100380	1.10.3.2 (Laccase)	GO:0016021;GO:0005743	integral component of membrane;mitochondrial inner membrane	N/A	N/A	GO:0006067	ethanol metabolic process	IPR007248	Mpv17/PMP22	PF04117	Mpv17/PMP22	N/A	N/A
Candida auris strain B8441	387	B9J08_000517	hypothetical protein	OG6_100257	1.10.3.2 (Laccase);1.10.3.3 (L-ascorbate oxidase);1.16.3.1 (Ferroxidase);1.7.2.1 (Nitrite reductase (NO-forming));2.7.-.- (Transferring phosphorus-containing groups.);3.2.1.- (Glycosidases, i.e. enzymes hydrolyzing O- and S-glycosyl compounds.);3.2.1.3 (Glucan 1,4-alpha-glucosidase);3.2.1.97 (Endo-a	GO:0033573	high-affinity iron permease complex	GO:0005507;GO:0004322;GO:0016491	copper ion binding;ferroxidase activity;oxidoreductase activity	GO:0006811;GO:0005072;GO:0055114;GO:0033215	ion transport;iron ion homeostasis;obsolete oxidation-reduction process;reductive iron assimilation	IPR001117;IPR002355;IPR008972;IPR011706;IPR011707;IPR033138	Multicopper oxidase, type 1;Multicopper oxidase, copper-binding site;Cupredoxin;Multicopper oxidase, type 2;Multicopper oxidase, type 3;Multicopper oxidases, conserved site	PF00394;PF07731;PF07732	Multicopper oxidase, type 1;Multicopper oxidase, type 2;Multicopper oxidase, type 3	SSF49503	Cupredoxin
Candida auris strain B8441	387	B9J08_002997	hypothetical protein	OG6_100257	1.10.3.2 (Laccase);1.10.3.3 (L-ascorbate oxidase);1.16.3.1 (Ferroxidase);1.7.2.1 (Nitrite reductase (NO-forming));2.7.-.- (Transferring phosphorus-containing groups.);3.2.1.- (Glycosidases, i.e. enzymes hydrolyzing O- and S-glycosyl compounds.);3.2.1.3 (Glucan 1,4-alpha-glucosidase);3.2.1.97 (Endo-a	GO:0016021	integral component of membrane	GO:0005507;GO:0016491	copper ion binding;oxidoreductase activity	GO:0006811;GO:0005072;GO:0051321;GO:0005114;GO:0070193	ion transport;iron ion homeostasis;meiotic cell cycle;obsolete oxidation-reduction process;synaptonemal complex organization	IPR001117;IPR002355;IPR008972;IPR011706;IPR011707;IPR033138	Multicopper oxidase, type 1;Multicopper oxidase, copper-binding site;Cupredoxin;Multicopper oxidase, type 2;Multicopper oxidase, type 3;Multicopper oxidases, conserved site	PF00394;PF07731;PF07732	Multicopper oxidase, type 1;Multicopper oxidase, type 2;Multicopper oxidase, type 3	SSF49503	Cupredoxin
Candida auris strain B11243	931	CJJ07_002884	unspecified product	OG6_100380	1.10.3.2 (Laccase)	GO:0016021	integral component of membrane	N/A	N/A	N/A	N/A	IPR007248	Mpv17/PMP22	PF04117	Mpv17/PMP22	N/A	N/A
Candida auris strain B11243	931	CJJ07_002885	unspecified product	OG6_100380	1.10.3.2 (Laccase)	GO:0016021	integral component of membrane	N/A	N/A	N/A	N/A	IPR007248	Mpv17/PMP22	PF04117	Mpv17/PMP22	N/A	N/A
Candida auris strain B11243	931	CJJ07_003625	unspecified product	OG6_100257	1.10.3.2 (Laccase);1.10.3.3 (L-ascorbate oxidase);1.16.3.1 (Ferroxidase);1.7.2.1 (Nitrite reductase (NO-forming));2.7.-.- (Transferring phosphorus-containing groups.);3.2.1.- (Glycosidases, i.e. enzymes hydrolyzing O- and S-glycosyl compounds.);3.2.1.3 (Glucan 1,4-alpha-glucosidase);3.2.1.97 (Endo-a	GO:0016021	integral component of membrane	GO:0005507;GO:0016491	copper ion binding;oxidoreductase activity	GO:0006811;GO:0005072;GO:0055114	ion transport;iron ion homeostasis;obsolete oxidation-reduction process	IPR001117;IPR002355;IPR008972;IPR011706;IPR011707;IPR033138	Multicopper oxidase, type 1;Multicopper oxidase, copper-binding site;Cupredoxin;Multicopper oxidase, type 2;Multicopper oxidase, type 3;Multicopper oxidases, conserved site	PF00394;PF07731;PF07732	Multicopper oxidase, type 1;Multicopper oxidase, type 2;Multicopper oxidase, type 3	SSF49503	Cupredoxin
Candida auris strain B11243	931	CJJ07_003902	unspecified product	OG6_100257	1.10.3.2 (Laccase);1.10.3.3 (L-ascorbate oxidase);1.16.3.1 (Ferroxidase);1.7.2.1 (Nitrite reductase (NO-forming));2.7.-.- (Transferring phosphorus-containing groups.);3.2.1.- (Glycosidases, i.e. enzymes hydrolyzing O- and S-glycosyl compounds.);3.2.1.3 (Glucan 1,4-alpha-glucosidase);3.2.1.97 (Endo-a	N/A	N/A	GO:0005507;GO:0016491	copper ion binding;oxidoreductase activity	GO:0006811;GO:0005072;GO:0055114	ion transport;iron ion homeostasis;obsolete oxidation-reduction process	IPR001117;IPR002355;IPR008972;IPR011706;IPR011707;IPR033138	Multicopper oxidase, type 1;Multicopper oxidase, copper-binding site;Cupredoxin;Multicopper oxidase, type 2;Multicopper oxidase, type 3;Multicopper oxidases, conserved site	PF00394;PF07731;PF07732	Multicopper oxidase, type 1;Multicopper oxidase, type 2;Multicopper oxidase, type 3	SSF49503	Cupredoxin

Supplementary Table 1. List of laccase homologues in C. auris from FungiDB

Organism	CDC. Strain	Gene ID	Product Description	Ortholog Group	EC numbers from OrthoMCL	Computed GO Component IDs	Computed GO Components	Computed GO Function IDs	Computed GO Functions	Computed GO Process IDs	Computed GO Processes	Interpro ID	Interpro Description	PFam ID	PFam Description	Superfamily ID	Superfamily Description
Candida auris strain B11220	381	CJI96_0000655	hypothetical_protein	OG6_105162	1.14.18.1 (Tyrosinase)	GO:0005789;GO:0016021	endoplasmic reticulum membrane;integral component of membrane	N/A	N/A	GO:0006629	lipid metabolic process	IPR005352	Erg28	PF03694	Erg28	N/A	N/A
Candida auris strain B11220	381	CJI96_0000674	hypothetical_protein	OG6_101780	N/A	GO:0016021	integral component of membrane	N/A	N/A	N/A	N/A	N/A	N/A	PF01544	N/A	SSF143865; SSF144083	CorA soluble domain-like; Magnesium transport protein CorA, transmembrane region
Candida auris strain B11220	381	CJI96_0003008	hypothetical_protein	OG6_101780	N/A	GO:0016021	integral component of membrane	N/A	N/A	N/A	N/A	N/A	N/A	PF01544	N/A	SSF143865; SSF144083	CorA soluble domain-like; Magnesium transport protein CorA, transmembrane region
Candida auris strain B11221	383	CJI97_001444	unspecified product	OG6_101780	N/A	GO:0016020	membrane	GO:0046873	metal ion transmembrane transporter activity	GO:0030001;GO:0055085	metal ion transport;transmembrane transport	IPR002523	Mg2+ transporter protein, CorA-like/Zinc transport protein ZntB	PF01544	Mg2+ transporter protein, CorA-like/Zinc transport protein ZntB	SSF143865; SSF144083	CorA soluble domain-like; Magnesium transport protein CorA, transmembrane region
Candida auris strain B11221	383	CJI97_002873	unspecified product	OG6_105162	1.14.18.1 (Tyrosinase)	GO:0005789;GO:0016021	endoplasmic reticulum membrane;integral component of membrane	N/A	N/A	GO:0006629	lipid metabolic process	IPR005352	Erg28	PF03694	Erg28	N/A	
Candida auris strain B11221	383	CJI97_002891	unspecified product	OG6_101780	N/A	GO:0016021;GO:0016020	integral component of membrane;membrane	GO:0046873	metal ion transmembrane transporter activity	GO:0030001;GO:0055085	metal ion transport;transmembrane transport	IPR002523	Mg2+ transporter protein, CorA-like/Zinc transport protein ZntB	PF01544	Mg2+ transporter protein, CorA-like/Zinc transport protein ZntB	SSF143865; SSF144083	CorA soluble domain-like; Magnesium transport protein CorA, transmembrane region
Candida auris strain B11245	386	CJJ09_001261	unspecified product	OG6_101780	N/A	N/A	N/A	N/A	N/A	N/A	N/A	N/A	N/A	PF01544	N/A	SSF143865; SSF144083	CorA soluble domain-like; Magnesium transport protein CorA, transmembrane region
Candida auris strain B11245	386	CJJ09_001280	unspecified product	OG6_105162	1.14.18.1 (Tyrosinase)	GO:0005789;GO:0016021	endoplasmic reticulum membrane;integral component of membrane	N/A	N/A	GO:0006629	lipid metabolic process	IPR005352	Erg28	PF03694	Erg28	N/A	N/A
Candida auris strain B11245	386	CJJ09_003418	unspecified product	OG6_101780	N/A	N/A	N/A	N/A	N/A	N/A	N/A	N/A	N/A	PF01544	N/A	SSF143865; SSF144083	CorA soluble domain-like; Magnesium transport protein CorA, transmembrane region
Candida auris strain B8441	387	B9J08_001162	hypothetical protein	OG6_101780	N/A	GO:0005886	plasma membrane	GO:0022890;GO:0046873	inorganic cation transmembrane transporter activity;metal ion transmembrane transporter activity	GO:0006812;GO:0015693;GO:0055085	cation transport;magnesium ion transport;transmembrane transport	N/A	N/A	PF01544	N/A	SSF143865; SSF144083	CorA soluble domain-like; Magnesium transport protein CorA, transmembrane region
Candida auris strain B8441	387	B9J08_002817	hypothetical protein	OG6_105162	1.14.18.1 (Tyrosinase)	GO:0005789;GO:0016021	endoplasmic reticulum membrane;integral component of membrane	GO:0030674	protein-macromolecule adaptor activity	GO:0070988;GO:0006696;GO:0006629	demethylation;ergosterol biosynthetic process;lipid metabolic process	IPR005352	Erg28	PF03694	Erg28	N/A	N/A
Candida auris strain B8441	387	B9J08_002836	hypothetical protein	OG6_101780	N/A	GO:0000329;GO:0016021;GO:1990816	fungal-type vacuole membrane;integral component of membrane;vacuole-mitochondrion membrane contact site	GO:0015095	magnesium ion transmembrane transporter activity	GO:0010961;GO:0030001;GO:0055085	cellular magnesium ion homeostasis;metal ion transport;transmembrane transport	N/A	N/A	PF01544	N/A	SSF143865; SSF144083	CorA soluble domain-like; Magnesium transport protein CorA, transmembrane region
Candida auris strain B11243	931	CJJ07_003398	unspecified product	OG6_105162	1.14.18.1 (Tyrosinase)	GO:0005789;GO:0016021	endoplasmic reticulum membrane;integral component of membrane	N/A	N/A	GO:0006629	lipid metabolic process	IPR005352	Erg28	PF03694	Erg28	N/A	N/A
Candida auris strain B11243	931	CJJ07_004279	unspecified product	OG6_101780	N/A	GO:0016020	membrane	GO:0046873	metal ion transmembrane transporter activity	GO:0030001;GO:0055085	metal ion transport;transmembrane transport	IPR002523	Mg2+ transporter protein, CorA-like/Zinc transport protein ZntB	PF01544	Mg2+ transporter protein, CorA-like/Zinc transport protein ZntB	SSF143865; SSF144083	CorA soluble domain-like; Magnesium transport protein CorA, transmembrane region
Candida auris strain B11243	931	CJJ07_004614	unspecified product	OG6_101780	N/A	GO:0016020	membrane	GO:0046873	metal ion transmembrane transporter activity	GO:0030001;GO:0055085	metal ion transport;transmembrane transport	IPR002523	Mg2+ transporter protein, CorA-like/Zinc transport protein ZntB	PF01544	Mg2+ transporter protein, CorA-like/Zinc transport protein ZntB	SSF143865; SSF144083	CorA soluble domain-like; Magnesium transport protein CorA, transmembrane region

Supplementary Table 2. List of tyrosinase homologues in C. auris from FungiDB